NTNU

Norwegian University of
Science and Technology

Design of a Counter Weight Suspension System for the TetraSpar Floating Offshore Wind Turbine

Brandon Thomas Pereyra

Wind Energy
Submission date: July 2018
Supervisor: Zhen Gao, IMT

Norwegian University of Science and Technology
Department of Marine Technology

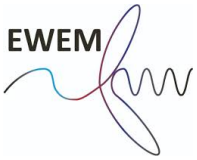

Design of a Counter Weight Suspension System for the TetraSpar Floating Offshore Wind Turbine

by

Brandon Thomas Pereyra
July 2018

Master Thesis
Delft University of Technology &
Norwegian University of Science and Technology

Supervisors: Zhen Gao, Riaan van 't Veer,
Morten Thøtt Andersen, Henrik Stiesdal, Zhiyu Jiang

Abstract

New floating wind turbine designs are needed to reduce production costs and to increase mass production feasibility. The TetraSpar floating wind turbine achieves these goals by being constructed using components highly suitable for standardization and industrialization. The design makes use of a suspended submerged counter weight to obtain a low center of gravity for the floating system, while also allowing a low draft during transport and installation. An analytic analysis of the counter weight suspension system is presented that investigates the behavior of the system. The main concern of the novel system is its motion relative to the upper floating platform which it is connected to. It is demonstrated that the suspended system's motion is described by the axial elongation of the suspension lines when positive tension is maintained in all suspension lines. An analytic solution for the equivalent stiffness of the suspension system is given. This suspension system stiffness introduces additional natural frequencies into the system, and the effects of these frequencies are demonstrated.

This novel concept requires a multibody modeling approach to perform a dynamic loads and response analysis, as the stiffness between the floating platform and the counter weight is provided by chains. Additional design criteria are required for the counter weight system dependent on a combination of chain capacity and maintaining positive tension in all of the suspension lines. To satisfy these design criteria a global hydrodynamic load and response analysis of the floating system is performed. In this concept, the counter weight depth contributes significantly to the dynamic properties of the system and therefore a parametric study is conducted. The global response parameters of the rigid-body motion, natural frequencies, nacelle accelerations, counter weight chain tensions, and maximum platform-pitch angles are compared. Following the parametric study, an ultimate limit state analysis is conducted on the original and alternative designs. Design recommendations are made for the counter weight depth and configuration of the suspension system layout.

Preface: Project Overview

The goal of this project will be to advance the development of the semi-submersible FOWT concept, the TetraSpar. The TetraSpar was developed by Stiesdal Offshore Technologies in an attempt to greatly reduce the cost of floating wind energy. There are several different organizations involved in the development of the TetraSpar FOWT. A modeling campaign was performed by the Technical University of Denmark (DTU) at the Danish Hydraulic Institute (DHI). Following this wave tank testing campaign, a grant was awarded to Stiesdal Offshore Technologies by the Danish Energy Agency as part of their Energy Technology Development and Demonstration Program (EUDP) through the project TetraSpar (Grant number 64017-05171).

As part of the EUDP grant project there are four separate organizations responsible for different concentrations of the project: Stiesdal Offshore Technologies, Danish Ingeniør Service (DIS), Seimens Gamesa Renewable Energy, and the University of Aalborg (AAU). Stiesdal Offshore Technologies is responsible for the organization of the project and identifying cost drivers of the design. DIS will be responsible for the structural design. Siemens Gamesa Renewable Energy will be responsible for adjusting the design to adapt to the constraints and costs of marine operations. The University of Aalborg will be responsible for the hydrodynamic and mooring design of the project.

This master's thesis project is part of an independent masters thesis written for the Technical University of Delft (TU Delft) and Norges Teknisk Naturvitenskapelige Universitet (NTNU) though the European Wind Energy Masters supervised by NTNU, TU Delft, AAU, and Stiesdal Offshore Technologies. This masters thesis work is done in support of the mooring design work that is being performed at the University of Aalborg. The main focus of this report will be on suspension system design through analytic, frequency-domain, and time-domain hydrodynamic analysis.

Table of Contents

List of Figures

List of Tables

Chapter 1

Introduction to Floating Offshore Wind Energy

The idea of large scale floating offshore wind energy was first proposed by Professor William E. Heronemus at the University of Massachusetts in 1972 [1]. After four decades of research and development, floating offshore wind technology has been successfully implemented in the form of a commercial offshore wind farm. Much research and development has been completed, however floating wind technology is still in the early stages of development. In 2009 the first floating offshore wind turbine (FOWT) prototype, the Hywind Spar, was installed [2]. Continuing with the development of this spar concept, Statoil built the first offshore floating wind farm, commissioned in 2017 off the coast of Scotland [3]. Another prototype moving the industry forward is the semi-submersible demonstration project, WindFloat, which wrapped up its first prototype campaign in 2016 after five years of operation. The prototypes mentioned have performed well and established that floating offshore wind technology is a viable technology for electricity generation [2].

With the technology proven, the main focus of the industry is now to decrease costs. As can be seen from the number of prototypes in the industry, there is no converged solution for floating support structures. The industry has two main mechanisms of driving down costs. These methods of cost reduction are up-scaling the turbine size and technological development. Since, floating wind turbines have the additional expense of the mooring system and the floating support structure, it is expected that the industry will push for even larger turbines to achieve an optimal balance of system costs [4]. Currently, fixed bottom founded wind turbines between 4.2-9.5 MW, are the featured turbines by the two market leaders in the offshore wind industry, Siemens Gamesa Renewable Energy and MHI Vestas Offshore Wind [5, 6, 7]. Full-scale offshore floating wind turbines are typically seen to be between 6-8 MW [8]. These floating turbines are installed in water depths of 50-200 meters, while the fixed offshore turbines are installed in water depths less than 50 meters[8].

The scientific community has developed open source turbines to advance wind turbine de-

velopment. A common reference turbine is the National Renewable Energy Laboratory's (NREL's) 5 MW turbine [9], which consists of three blades, a rotor, nacelle, and tower. The NREL 5 MW turbine has a hub height of 90 meters, a rotor diameter of 126 meters, and a total mass of 697 tonnes. The Danish Technical University 10 MW Reference Wind Turbine (DTU 10 MW RWT) represents a theoretical turbine that was developed to help advance the development of even larger turbines [10]. The DTU 10 MW RWT turbine also consists of three blades, a rotor, nacelle, and tower. The DTU 10 MW RWT has a hub height of 119 meters, a rotor diameter of 178.3 meters, and a total mass of 1243 tonnes. Comparing these two turbines gives the impression that weight can scale linearly with power which demonstrates that it is attractive to build larger turbines to balance the total system costs.

Figure 1.1: The three main floating wind turbine concepts: the spar (left), semi-submersible (center), and tension leg platform (right). Illustration by Josh Bauer, NREL.

The main three types of floating support structures are the spar, semi-submersible, and tension leg platform (TLP) seen in Figure 1.1. These three concepts achieve stability in different ways. The TLP achieves stability through the mooring lines. To achieve stability, force is transmitted from the sea floor, through the mooring lines, and to the platform. These systems rely on embedded anchors to support large vertical forces. The spar floating platform achieves stability through ballast. This ballast lowers the center of gravity. The center of mass of the spar is positioned far below the center of buoyancy which provides a stabilizing moment [1].

Like the spar concept, the semi-submersible concept can also have a center of gravity

below the center of buoyancy, however the semi-submersible design relies on a large water plane area and inertia to provide stability. The semi-submersible support structure uses its weighted water-plane area to provide stability. Stability is achieved since a volume of the floating platform exits the water during pitch rotation; as volume exits the water plane this decreases the buoyancy force on that side of the platform. Conversely the buoyancy force increases in the side rotating into the water as volume is submerged. This increase of buoyancy on the submerged side and decrease in buoyancy on the lifting side causes a buoyancy restoring moment [1].

1.1 Mooring

A mooring system is required for any floating offshore wind turbine. The purpose of a mooring system is to limit the FOWT's position in surge, sway, and yaw within a certain position range. The limits to surge and sway excursion are determined by the following requirements: to keep the turbines within the permitted space, to avoid collision with neighboring turbines, to avoid excessive stretching of the electrical cable connections, and to avoid contributing to a system stiffness that results in resonance at any degree-of-freedom.

In addition to resisting horizontal forces, the mooring system must operate under dynamic wave and wind conditions which cause cyclic dynamic tensions. The dynamic tensions caused by first-order wave forces are cyclic, As cyclic forces result in zero average motion it is not necessary to control the dynamic motion caused by the first-order wave forces. From this reasoning, it is beneficial to have a compliant mooring system that produces a restoring force to resist the horizontal mean environmental forces, but has a low enough stiffness to minimize dynamic tensions.

There are three types of mooring systems: taut, catenary, and tension. The three variants of mooring designs are displayed in Figure 2.3.

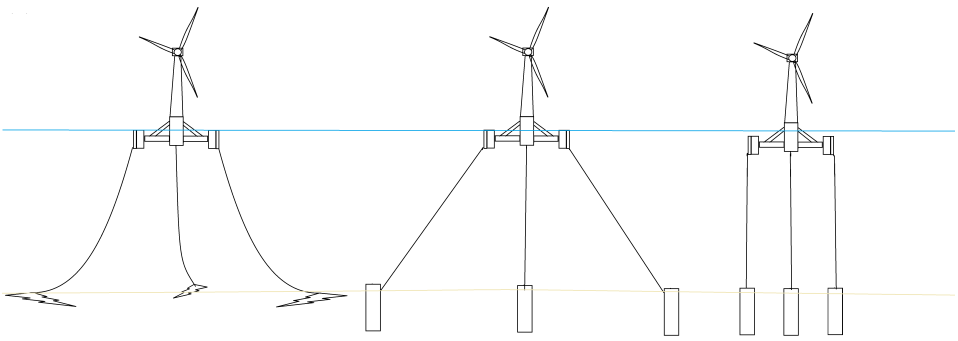

Figure 1.2: Mooring systems types: catenary (left), taut (center), and tension (right).

A taut mooring system connects the floating platform directly to the anchor using straight mooring lines. Taut mooring systems provide restoring forces from the elastic modulus of the mooring line material (typically polyester). The anchor of a tension mooring system must be designed to handle large vertical and horizontal loads. For this reason, the taut mooring system typically uses pile anchors. Taut mooring systems require a pre-tension so that the tension in the mooring lines is large enough to remain straight and provide the proper restoring force. Special mooring installation vessels are required to perform this pre-tensioning operation. It is important to consider that this pre-tensioning process would not only have to be done during the initial installation, but also after maintenance, in the case that the turbine is detached and brought back to a port for repairs. An advantage of the taut mooring system is that it can be used to reduce the footprint of a mooring system.

Tension leg mooring systems are mooring lines that connect the floating system with the sea floor using vertical lines. The stability of this system is provided by the large vertical forces in the mooring lines; these tensions keep the floating platform in place despite its large buoyancy force. In a tension leg platform, small displacements in surge and sway resulting in large restoring forces. This mooring design results in the smallest mooring footprint possible.

There are three main mooring line types used to construct the mooring system. The mooring lines are typically composed of some combination of the following: chain link, steel wire, or synthetic fiber. The material properties are what differentiate these line types. The main material properties of importance are ultimate tensile strength, axial stiffness, and weight [11].

The catenary mooring system connects the anchor and floating platform together with a hanging line. The catenary line is designed with more line length than a straight line connecting the platform and the anchor, see Figure 2.15, causing the line to hang due to self weight. The catenary line has enough slack in the line to allow it to hang freely with part of it laying on the sea floor. Catenary mooring systems maintain equilibrium using the principal catenary action. When the turbine moves out of the equilibrium position, one mooring line is stretched in tension as the distance between the platform and anchor increases. This causes part of the mooring line to lift off the sea floor. This weight of the additional suspended mooring line causes an increase in line tension which provides a restoring force. The opposite happens to the mooring line on the side opposite the motion, a decrease in distance causes more mooring line to rest on the sea floor leading to a reduction in weight and line tension. The described geometric relationship results in a non-linear geometrical problem. Since the stiffness of a catenary mooring system is non-linear, it is important to consider the influence on the stiffness of the system at it's maximum excursion as well as zero excursion.

Chapter 2

Theory

2.1 Hydrostatic

Floating bodies maintain their equilibrium about the mean water line through displaced water volume Eqn. (2.1). This buoyancy force, F_B offsets the weight of the body. If an external force acts on the floating body, equilibrium would be achieved when additional volume, V, was submerged below the water to balance this external force. In Eqn. (2.1), the gravitational constant is given by g and density of water by ρ.

$$F_B = \rho g V \tag{2.1}$$

Floating support structures must be able to resist environmental forces. This is achieved through the bodies hydrostatic stiffness. The formula for hydrostatic heave stiffness is given in Eqn. (2.2) [12]. The area of the body that intersects the water plane is called the water plane area, A_{WP}, it provides the stiffness for the body in heave. This stiffness is a function of body geometry and changes with the changing area intersecting the water plane. It is common to approximate the stiffness of a body using the water plane area for the body in the undisturbed position, $A_{WP}(0, 0, 0)$, in reality the stiffness term is non-linear for many designs. The average stiffness over the expected range of motion can give a better approximation of the stiffness.

$$C_{33} = \rho g A_{WP}(z, \phi, \theta) \tag{2.2}$$

The formula for hydrostatic pitch stiffness is given in Eqn. (4.1) [12]. The ability of a floating structure to resist an overturning moment is provided by its stiffness in pitch. The stiffness is provided by the restoring moments of the gravitational force and buoyancy force. The center of gravity (CoG) of the body is fixed, but the center of buoyancy (CoB)

is not and changes with changes in the displaced water volume. Eqn. (4.1) represents the CoB using a constant and variable term. The constant term is the CoB at the body's undisturbed position and the variable term contains an integration of the second moment of area about the water plane area. All of the terms in Eqn. (4.1) are non-linear and make assumptions using the small angle approximation.

The metacentric height, $\overline{GM}$, is commonly used as a measure of stability for a floating body. The metacentric height can change with varying angles of pitch. Figure 2.1 shows the metacentric height for a spar floating body. Since the water plane area is small, the difference is small between the undisplaced center of buoyancy, B, and the shifted center of buoyancy, B'. As a result the metacentric height of a floating body, with a small water plane area, can assumed to be constant and related to the distance between the undisplaced center of gravity and center of buoyancy.

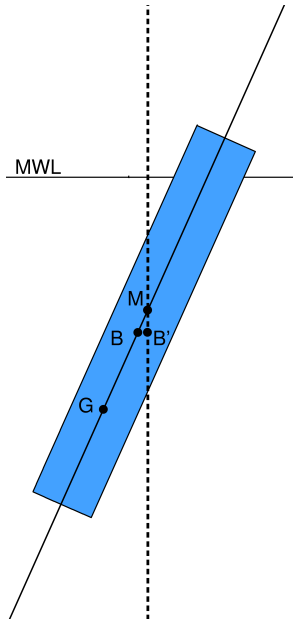

Figure 2.1: The metacentric height is given by the distance from the center of gravity to the metacenter of the body.

$$C_{55} = \rho g V(CB - CG) + \rho g \iint_{A_{WP}} x^2 ds = \rho g V \overline{GM} \tag{2.3}$$

$$C_{55} = B_P CB_P - W_P CG_P + (B_{CW} - W_{CW}) CG_{CW} - W_T CG_T \tag{2.4}$$

2.2 Linear Airy-Waves

Wave loading is caused by the pressure field that waves create as they interact with floating bodies. Faltinsen [12] describes the dynamic pressure field in Eqn. (2.6). This dynamic pressure field is assumed to be created by a regular wave described by (2.5).

$$\zeta = \zeta_a sin(\omega t - kx) \tag{2.5}$$

Where ζ_a is the wave amplitude, ω is the wave frequency, and k is the wave number. The pressure is dependent on depth and depends on water depth (h), on water density (ρ), and on the gravitational constant (g).

$$p_D = \rho g \zeta_a \frac{cosh(k(z+h))}{cosh(kh)} sin(\omega t - kx) \tag{2.6}$$

2.3 Frequency- and Time-Domain Hydrodynamics

For motion to occur in a fluid, a floating body must change the pressure field of the fluid that it is submerged in. The alteration of this fluid field can be described using Bernoulli's equation and velocity potential. It is assumed that water is incompressible, inviscid, and that any fluid motion is irrotational. The mentioned assumptions form the basis of hydrodynamic analysis and result in the Laplace equation (2.7).

$$\frac{\partial^2 \phi_v}{\partial x^2} + \frac{\partial^2 \phi_v}{\partial y^2} + \frac{\partial^2 \phi_v}{\partial z^2} = 0 \tag{2.7}$$

The hydrodynamic system can be modeled in the time-domain or frequency-domain starting from the dynamic equations of motion. It is assumed that the floating structure can be modeled as a rigid body with 6 DOF. The validity of this assumption comes into question since the TetraSpar design consists of a two-body system that is connected using suspension lines. If the stiffness of these suspension lines is significantly small, then additional DOF will be introduced. The equation representing the floating wind turbine motion in the time-domain is written in Eqn. 2.13 followed by the frequency-domain equation of motion written in Eqn. 2.8 [13].

$$-\omega^2(\bar{\bar{\mathbf{M}}} + \bar{\bar{\mathbf{A}}}(\omega))X(\omega) + i\omega\bar{\bar{\mathbf{B}}}(\omega)X(\omega) + \bar{\bar{\mathbf{C}}}X(\omega) = \bar{\bar{\mathbf{F}}}_{exct}(\omega) \tag{2.8}$$

Where $\boldsymbol{X}$ represents the motion in 6 DOF. The other terms include the added-mass of the structure $\bar{\bar{\mathbf{A}}}$, the potential damping $\bar{\bar{\mathbf{B}}}$, the system stiffness $\bar{\bar{\mathbf{C}}}$, and the wave excitation

force $\bar{\bar{\mathbf{F}}}_{exct}$. The added-mass and potential damping of the structure are both dependent on the frequency of the wave forcing. From this frequency-domain analysis the added-mass, potential damping, and force excitation function will be reported. These variables can be used to determine the transfer function. The transfer function expresses the relationship between a unit wave and displacement it causes based on frequencies. These RAOs are used to analyze the response of the system over different frequencies. The RAO can be used to determine the natural frequencies of the system, the maximum response amplitude, and the effects of damping on the system.

$$RAO(\omega) = X(\omega) = [-\omega^2(\bar{\bar{\mathbf{M}}} + \bar{\bar{\mathbf{A}}}(\omega)) + i\omega\bar{\bar{\mathbf{B}}}(\omega) + \bar{\bar{\mathbf{C}}}]^{-1}\bar{\bar{\mathbf{F}}}_{exct}(\omega) \tag{2.9}$$

It is also possible to model the structure in the time-domain. Moving from the frequency-domain to the time-domain requires frequency dependant information to be accounted for in a different way. By splitting the frequency dependant added-mass term up, into a constant term and a frequency dependent added-mass term, then computing the inverse Fourier transform, the dynamic frequency-domain equation can be converted into the time domain as done in Equations 2.10 and 2.11 [13].

$$\mathbf{A}(\omega) = \mathbf{A}_\infty + a(\omega) \tag{2.10}$$

$$(\bar{\bar{\mathbf{M}}} + \bar{\bar{\mathbf{A}}}_\infty)\ddot{\boldsymbol{X}}(t) + \int_{-\infty}^{\infty}(i\omega a(\omega) + B(\omega))i\omega\boldsymbol{X}(\omega)\exp i\omega t d\omega + \bar{\bar{\mathbf{C}}}\boldsymbol{X}(t) = \boldsymbol{F}(t) \tag{2.11}$$

The convolution integral can be used to represent the integration term in Equation (2.11) in the time-domain, as seen in Equation (2.12) [13].

$$(\bar{\bar{\mathbf{M}}} + \bar{\bar{\mathbf{A}}}_\infty)\ddot{\boldsymbol{X}}(t) + \int_{-\infty}^{\infty}k(t-\tau)\boldsymbol{X}(\tau)d\tau + \bar{\bar{\mathbf{C}}}\boldsymbol{X}(t) = \boldsymbol{F}(t) \tag{2.12}$$

Equation (2.12) represents the equations of motion in the time-domain while considering the effects of radiation damping dependent on frequency. In addition to modeling damping in the time-domain using the convolution integral, constant coefficients can also be used to represent linear and quadratic damping giving Equation 2.13.

$$(\bar{\bar{\mathbf{M}}} + \bar{\bar{\mathbf{A}}}_\infty)\ddot{\boldsymbol{X}}(t) + \bar{\bar{\mathbf{B}}}\dot{\boldsymbol{X}}(t)\left|\dot{\boldsymbol{X}}(t)\right| + \bar{\bar{\mathbf{B}}}\dot{\boldsymbol{X}}(t) + \bar{\bar{\mathbf{C}}}\boldsymbol{X}(t) = \boldsymbol{F}(t) \tag{2.13}$$

The benefit of using the time-domain is that non-linear effects are accounted for. Non-linear effects arise from multiple sources. The forces from the mooring lines are non-linear due to geometry, material, and boundary-condition effects. The drag forces responsible for damping in the system are also non-linear. The drag force on a cylinder of unit length can

be approximated using the Morison Equation 2.14 [12]. The left-hand side of Morison's equation represents the force contribution due to drag and the right-hand side represents the force contribution due to inertia.

Moving to the time-domain from the frequency-domain requires that the frequency dependant information is accounted for in a different way. To account for the frequency dependant information in the time-domain a convolution integral is performed across time.

$$F_{wave} = \frac{1}{2}\,\rho \cdot C_D \cdot D\ |U|\,U + \rho \cdot C_M \cdot A \cdot \frac{dU}{dt} \tag{2.14}$$

Both first-order and second-order wave loads are important in the design of a offshore floating support structures. The first-order loads act on the structure at the same frequency of the waves which cause the loads. The second-order loads introduce loading at two frequencies: the sum- and difference-frequency. The sum-frequency acts at higher weave frequencies of twice the wave frequency and the difference-frequency results in forces which occur at lower frequencies [14]. For spar structures it was demonstrated by Roald [15] that second-order forces are small compared to first-order wave forces. Although the second-order forces are small in magnitude compared to first order forces, they are still important to analyze because their forcing can occur at the excitation frequencies of the structure. Typically offshore floating structures are designed with low natural frequencies in all degrees-of-freedom. This is done so that the natural frequencies of the system do not overlap with the first-order wave forcing. Even if the structure's natural frequencies avoid the first-order frequencies, they can be excited by these second-order frequencies. The second-order low frequency motions are especially important for mooring design since mooring systems typically have low natural frequencies [15].

In the present study of the TetraSpar, second-order wave effects are ignored. It is possible that second-order effects are of importance, however this initial investigation will first focus on first-order effects. The second-order solution is time consuming and requires additional discretization of the free surface. As this study focuses on the counter weight suspension system, pitch and roll motion is expected to have the greatest influence on the design. Results from Roland [15] demonstrate that first-order wave forces dominate the force and motion response in the pitch degree-of-freedom. For these reasons only first-order wind, wave, and current forces are considered.

2.4 Catenary Mooring Equations

In a catenary mooring cable the displacement and stiffness in the vertical direction is assumed to be negligible. Faltinsen provides the following equations that can be used to describe the line tension in a catenary mooring cable [12]:

$$dT - \rho g A dz = [w sin(\phi) - F(1 + T/(AE))]ds \tag{2.15}$$

$$Td\phi - \rho g A z d\phi = [w cos(\phi) + D(1 + T/(AE))]ds \tag{2.16}$$

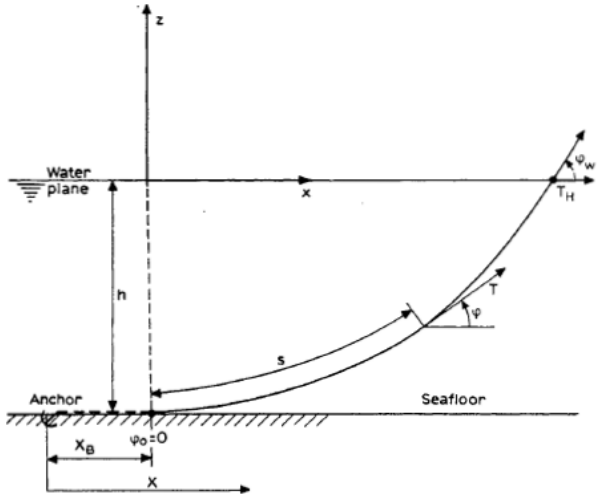

Figure 2.2: Basic mooing line geometry with excess line to produce a slack chain or cable from Faltinsen.

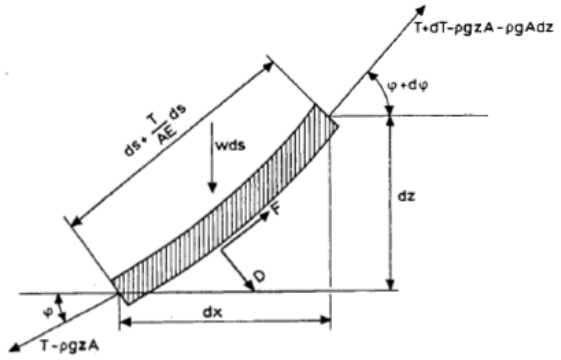

Figure 2.3: Discretized element of a mooring line from Faltinsen.

If we assume that the effects of current and elasticity on mooring line tension can be ignored, the following simplified equations can represent the non-linear geometrical force-

displacement relationship of a catenary mooring system [12].

$$T' = T - \rho g z A \tag{2.17}$$

If a relationship between change in tension and weight is made, then by integrating Equations 2.15 and 2.17 the following equations can be derived to describe a non-elastic catenary system. Figure 2.4 displays the variables L, L_s, x, h, and X which repectivly represent line length, lifted line length, horizontal distance from the fairlead to the point of mooring line contact with the sea floor, fairlead height, and total horizontal distance from the fairlead to the anchor. These variables are used in the following catenary equation derivations [12].

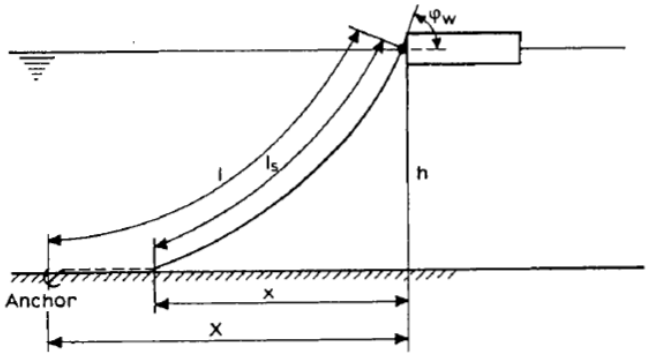

Figure 2.4: A catenary mooring system showing geometric line variables from Faltinsen.

The horizontal distance between the contact of the catenary system with the sea floor and the fairlead is given:

$$x = \frac{T_H}{w} cosh^{-1}(1 + \frac{wh}{T_H}) \tag{2.18}$$

The lifted line length, L_s, is given as a function of the horizontal force:

$$L_s = z(1 + 2\frac{T_H}{hw})^{\frac{1}{2}} = \frac{T_H}{w} sinh(\frac{wx}{T_H}) \tag{2.19}$$

The horizontal, vertical tension, and total tension are given by T_H, T_V, and T. The horizontal tension can then be given as a function of the lifted line length. As the lifted line length is a function of the horizontal tension, the horizontal tension can be expressed as a function of x and solved for using numerical methods.

$$T_H = \frac{hw}{2}((\frac{L_S}{2})^2 - 1) \tag{2.20}$$

$$T_V = wL_S \tag{2.21}$$

$$T = (T_H^2 + T_V^2)^{\frac{1}{2}} \tag{2.22}$$

To calculate the total distance from the anchor point to the fairlead the total unstretched length of the line, L, is used.

$$X = L - L_s + x = L - h(1 + 2\frac{T_H}{zw})^{\frac{1}{2}} + \frac{T_H}{w}cosh^{-1}(1 + \frac{wh}{T_H}) \tag{2.23}$$

Once the horizontal and vertical force displacement relationship is known for a single line, the one dimensional stiffness maxtrix can be calculated. These one dimensional stiffness matrices can then be combined to create a equivalent mooring system stiffness in 6DOF as outlined by Al-Solihat [16]. To calculate the 2D stiffness matrix K^{2D} for one line the 2D flexibility matrix, F, is inverted.

$$K^{2D} = \begin{bmatrix} K_{11}^{2D} & K_{12}^{2D} \\ K_{21}^{2D} & K_{22}^{2D} \end{bmatrix} = F^{-1} = \begin{bmatrix} \frac{\partial X}{\partial T_H} & \frac{\partial X}{\partial T_V} \\ \frac{\partial h}{\partial T_H} & \frac{\partial h}{\partial T_V} \end{bmatrix}^{-1} \tag{2.24}$$

$$\frac{\partial X}{\partial T_H} = \frac{1}{w}[\frac{-T_V}{\sqrt{T_H^2 + T_V^2}} + sinh^{-1}(\frac{T_V}{T_H})], \tag{2.25}$$

$$\frac{\partial X}{\partial T_V} = \frac{\partial h}{\partial T_H} = \frac{1}{w}[\frac{T_H}{\sqrt{T_H^2 + T_V^2}} - 1], \tag{2.26}$$

$$\frac{\partial h}{\partial T_V} = \frac{1}{w}[\frac{T_V}{\sqrt{T_H^2 + T_V^2}}] \tag{2.27}$$

It will be desired to know the mooring stiffness at zero surge displacement and at the maximum surge displacement. The mooring stiffness at zero surge displacement is given by Al-Solihat [16]. Where n is the number of mooring lines, R is the radius from the center

of the floating platform to the fairlead, and D is the vertical distance from the MWL to the fairlead. These stiffness can be used in a preliminary design check to account for the stiffness of the mooring system when designing a system that avoids the natural frequencies of environmental conditions. The following equations represent the equivalent mooring stiffness for zero surge displacement.

$$K_{11} = \frac{1}{2} n[K_{11}^{2D} + \frac{T_H}{X}] \quad (2.28)$$

$$K_{22} = \frac{1}{2} n[K_{11}^{2D} + \frac{T_H}{X}] \quad (2.29)$$

$$K_{33} = nK_{22}^{2D} \quad (2.30)$$

$$K_{44} = K_{55} = n[-DRK_{12}^{2D} + \frac{D^2}{2} K_{11}^{2D} + \frac{R^2}{2} K_{22}^{2D} + DT_V + RT_H + \frac{D^2 T_H}{2X}] \quad (2.31)$$

$$K_{66} = K_{55} = n[\frac{T_H R^2}{X} + T_H R] \quad (2.32)$$

Numerically the surge stiffness is also found for extreme excursions to check the system's natural frequency at these extreme excursions. During an excursion in extreme conditions, current, wind, and wave drift forces can give the floating system a mean excursion from the undisplaced position. The critical mooring line configuration to investigate is outlined by Bergdahl [17]. The direction of the critical environmental forcing for the mooring system is depicted in Fig. 2.5.

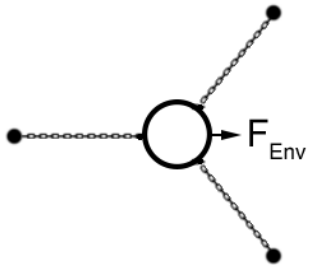

Figure 2.5: The critical direction of environmental forcing that results in the most extreme mooring line stiffness.

Variations in the maximum average environmental forcing will result in different mean offsets and different equivalent system stiffness. It is important to investigate this offset mooring stiffness as the increased stiffness in surge can increase the natural frequency of the system in surge bringing it closer to the frequencies of the wave spectrum. The 6 DOF stiffness can be calculated for the stretched and shortened lines individually and then

added together. The 6 DOF stiffness for individual lines is presented by Al-Solihat [16].

The surge displacement can be given as a function of the initial horizontal mooring line tension and the present mooring line tension as seen in Equation 2.33. This is a useful equation as it can be used in initial design calculations to check that the maximum static surge displacement is not exceeded for a given design load.

$$\delta = z(1 + 2\frac{T_{H_0}}{wz})^{\frac{1}{2}} - z(1 + 2\frac{T_{H_1}}{wz})^{\frac{1}{2}} + \frac{T_{H_1}}{w}cosh^{-1}(1 + \frac{wz}{T_{H_1}}) - \frac{T_{H_0}}{w}cosh^{-1}(1 + \frac{wz}{T_{H_0}}) \tag{2.33}$$

Chapter 3

The TetraSpar Floating Wind Support Structure

3.1 Summary

The TetraSpar floating wind turbine developed by Stiesdal Offshore Technologies A/S consists of several innovative concepts proposed by Stiesdal [18]. This report will focus on the new technology proposed: the multi-body support structure and the counter weight suspension system. In this chapter these concepts are first discussed, followed by a geometrical description of the design. The remainder of the report performs a technical investigation to demonstrate the physical behavior and design limits of each technology. For the two-body system, the design is driven by the separate hydrodynamic stability requirements of each body during transportation and installation. The hydrodynamic stability is discussed in the next chapter. For the counter weight suspension system, the design requirements are related to maintaining positive line tension in all of the suspension lines. The design of a counter weight suspension system is first discussed analytically. After the physical behavior of the suspension system is demonstrated, then a parametric study is performed using numerical simulations. The goal of the parametric study is to demonstrate a design process that can be used to design the suspension system. In this parametric study the ideal distance between the floating platform and counter weight is determined. Finally, an ultimate limit state check is performed to determine if the design processes has resulted in a successful design or if another design loop is required.

There are two main variations of the TetraSpar: an academic version designed for the DTU 10 MW reference wind turbine (RWT) and a 3.5 MW demonstration project. The 1:60 model-scale of the academic version of the TeteraSpar was tested at DHI by DTU [19]. It will be the academic version of the TetraSpar which is discussed and analyzed in this paper. In this chapter three variations of the academic version of the TetraSpar are described: the original design and two alternative designs. The two alternative designs were selected from the parametric study and designed to meet the requirements of hydrodynamic stability.

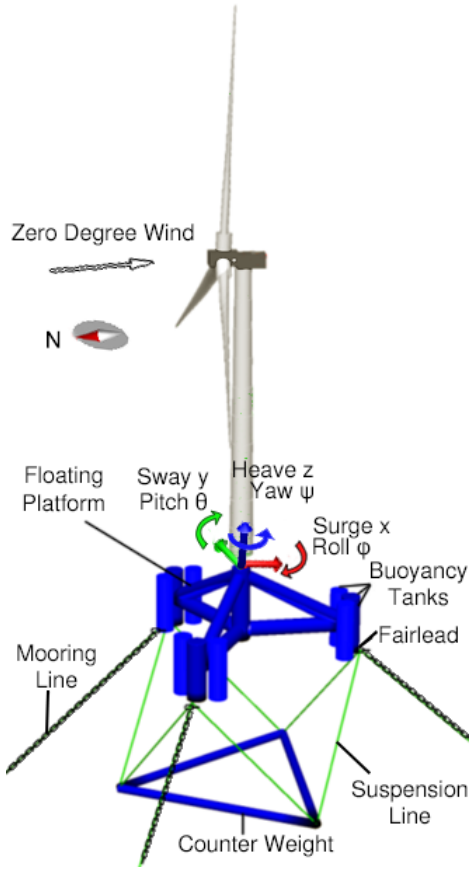

Figure 3.1: Global direction convention and main components of the TetraSpar with submerged members shown in blue.

3.2 TetraSpar Concept

Many floating offshore support structures have been proposed for wind turbines falling under the usual classifications of spar, semi-submersible, or tension leg platforms as outlined by Andersen [8]. The support structure investigated in this paper (Fig. 3.1) is unique in that its hydrostatic properties during operation are classified as a spar, but during transportation and installation are classified as a semi-submersible, see Fig 3.2. In the semi-submersible transportation phase, the hydrostatic stiffness in pitch is provided by the design's water plane area. Spar structures are classified as having hydrostatic stiffness in pitch mainly provided by the difference between the center of buoyancy (COB) and the center of gravity (COG). In the presented design's operational phase it meets the classification of a spar, as only the central members intersect with the water plane and all tanks are submerged below the mean water line (MWL); see the ballast counter weight configuration in Fig. 3.2.

The TetraSpar prioritizes the ability to be industrialized. In addition to its ability to be industrialized, there is additional innovation included in the concept that allows for the design to have a greater distance between the center of buoyancy and center of gravity compared to a conventional spar. This innovation, shown in Fig. 3.1, is a suspended keel which acts as a counter weight for the system to provide it with stability [18].

Traditional spars are limited, by their ability to be installed, due to their large drafts ranging from 80-120 m for 5-10 MW turbines [20, 21, 22]. The design of the TetraSpar enables it to have a small draft during installation. The draft of the original version of the TetraSpar designed for the DTU 10 MW Reference Wind Turbine (RWT) is 11 m during the transportation and installation phase and 82 m during normal operation. The ability to have separate drafts is achieved by being composed of two separate bodies: an upper floating platform and a suspended counter weight; see Fig. 3.2. These two bodies are connected together using suspension lines made of chain or synthetic rope. During the transportation and installation phase the floating platform of the TetraSpar acts as a semi-submersible platform and obtains its hyrdostatic stability primarily through water plane area, while the counter weight can be towed as a separate floating body.

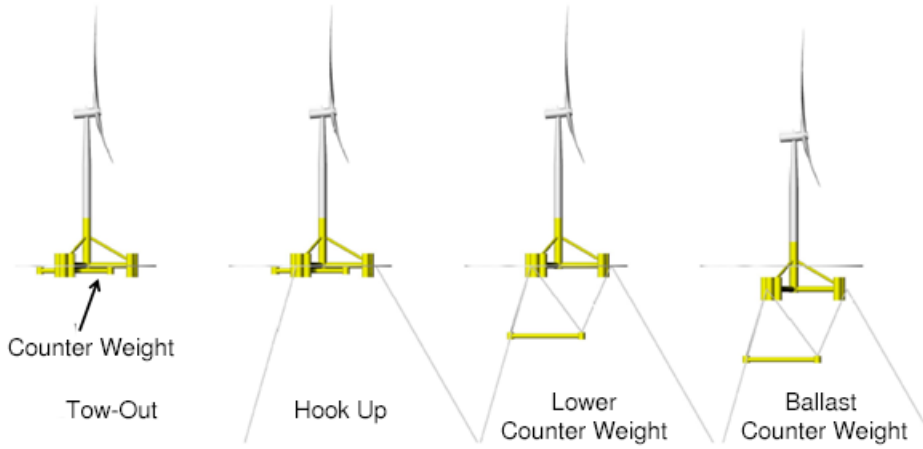

Figure 3.2: A possible installation procedure for the TetraSpar floating offshore wind turbine.

The first phase of installation allows for the mating of the wind turbine and floating platform to be performed at the quay site. The counter weight is able to float when its buoyancy compartments have not been flooded, this allows for the counter weight to be transported into the water separately. Once both bodies are in the water the suspension lines can be attached to connect the bodies together. With both bodies connected together they can be towed to the site of installation; see Fig. 3.2. At the site of installation or once the design has entered deep enough water, buoyancy compartments can be flooded allowing the design to transition into its spar configuration.

The suspended counter weight has been designed in such a way that there are six lines

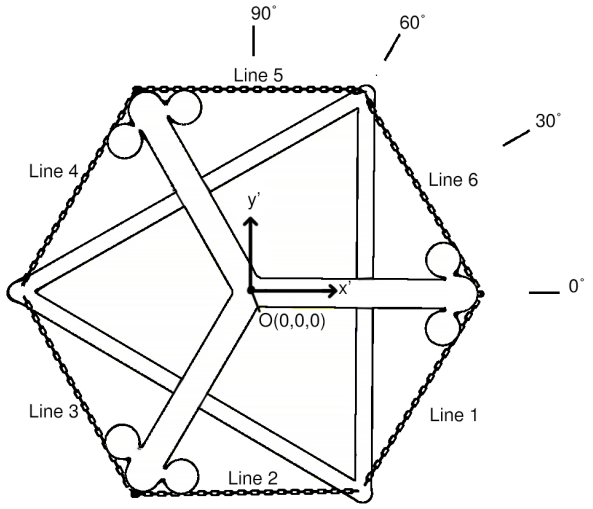

Figure 3.3: Top view of the TetraSpar.

connecting to six fairleads, three fairleads on the floating platform and three on the suspended counter weight, as shown in Fig. 3.1 and 3.3. In this system the counter weight is statically determined with little relative motion between it and the floating platform. A description of the counter weight and an explanation of the physics behind this statically determined multi-body system is given in the design and analysis of the counter weight suspension system.

The dimensions of the TetraSpar are taken from the first iteration of the 1:60 model scale designed for the DTU 10MW RWT. The dimensions of this model were scaled to the full scale values using Froude scaling. The 1:60 model was tested at the DHI wave basin[23]. From the tests performed and reported by DTU, a numerical model was built and calibrated in HydroD and SIMA.

3.3 TetraSpar Original and Alternative Model Dimensions

The TetraSpar floater is comprised two sections: a floating platform and a counter weight, seen in Figure 3.4. The upper floating platform is attached to the turbine at the top of the center column. The floating platform is also attached to the mooring lines at the end of the radial tube using a fairlead. The counter weight is attached to the platform using a fixed amount of chain. The main dimensions of the floating structure are provided in Figure 3.5. The components used to build the model scale structure are provided in Table 3.1 along with an approximated weight.

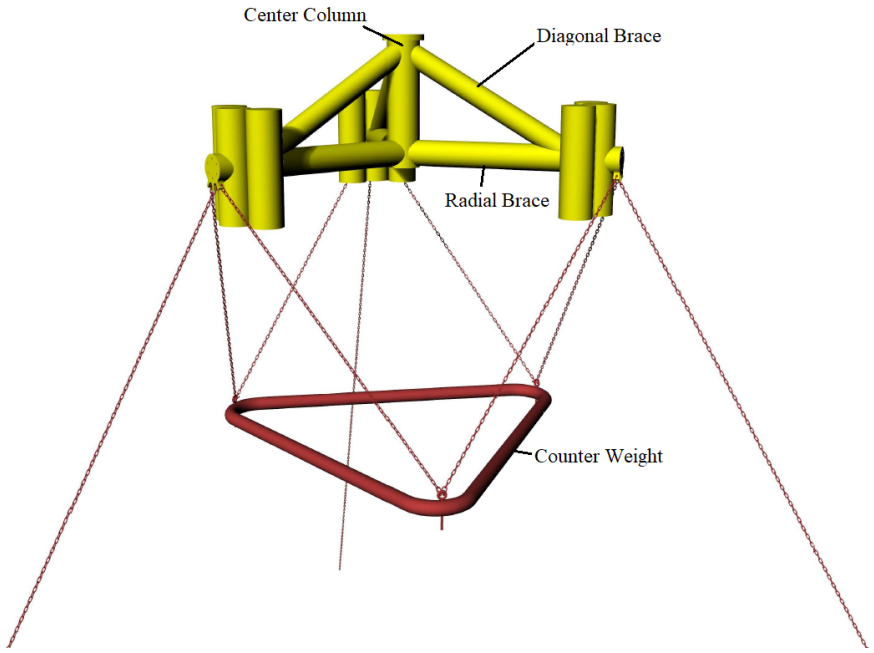

Figure 3.4: Perspective view of the TetraSpar floating wind turbine provided by Stiesdal Offshore Technologies.

The floating platform is designed to provide sufficient buoyancy to the system, to counteract the gravitational force of the system, allowing it to float. In the original design, the platform consists of a center column, three radial braces, three diagonal braces, and nine buoyancy tanks.

The counter weight is designed to stabilize the system by decreasing the center of gravity in the heave direction. The lower the center of gravity relative to the center of buoyancy the greater the stability of the system.

The dimensions of the counter weight in the original model were not supplied and assumed. The following counterweight was designed to be made out of steel with a density of 7800 kg/m^3. The counter weight is 58.2 meters in length with an outer diameter of 3 meters and a thickness of 75 millimeters.

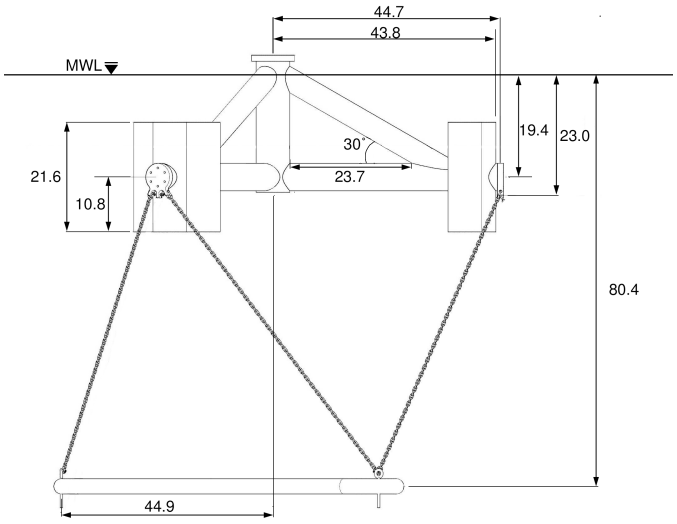

Figure 3.5: Dimensions for the original TetraSpar design given in meters.

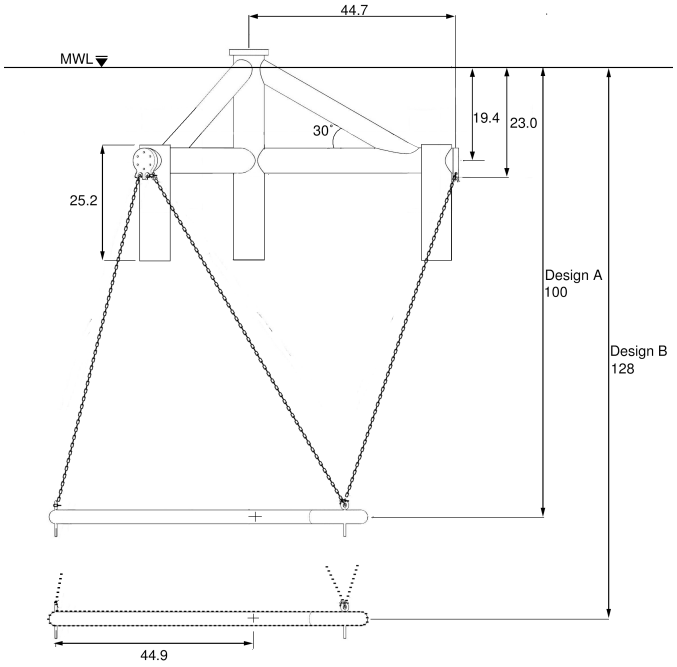

Figure 3.6: Dimensions for the alternative TetraSpar Designs A & B given in meters. The only difference between Design A and Design B is the position of the counter weight.

The dimensions of the floating platform for the original and alternative designs are shown in Fig. 3.5 and 3.6. Figure 3.5 shows the original design of the 1:60 model scale turbine tested at DHI by DTU. Figure 3.6 shows the modified Designs A & B of the TetraSpar presented in this study. As will be discussed in following sections the main goal of the design modification was to reduce the weight of the floating support structure. To do this, six of the buoyancy tanks were removed and the mass of the counter weight was decreased. The depth of the counter weight was increased to maintain operational stability. The tanks were also lowered in addition to adding a buoyancy tank below the center column. These modifications were made to improve the stability of the upper floating platform during its transportation and installation phase.

Part No.	Part	Material (m)	No.	Mass/Piece (tonnes)	Mass/Set (tonnes)	Total (tonnes)
1	Complete Model		1			3572
2	Complete Center Column		1		369.4	369.4
2.1	Center Tube	Steel, ø6.6/6.478 x 30	1	283.0	283.0	
2.2	Base Plate	Steel, ø6.216 x 0.059	1	13.0	13.0	
2.3	Transition Flange	Steel, ø8.64/7.89 x 1.2	1	73.4	73.4	
3	Complete Radial Brace		3		304.5	913.5
3.1	Radial Tube	Steel, ø5.4/5.3 x 42.3	1	267.8	267.8	
3.2	Radial End Cap	Steel, ø5.076 x 0.235	1	36.7	36.7	
4	Complete Diagonal Brace		3		205.6	616.8
4.1	Diagonal Tube	Steel, ø4.5/4.369 x 37.5	1	250.6	205.6	
5	Complete Tank Set		3		443.1	1329.3
5.1	Center Tank	Steel, ø6.6/6.525 x 21.6	1	110.2	110.2	
5.2	Side Tank	Steel, ø6.6/6.525 x 21.6	2	127.4	254.9	
5.3	Base Plate	Steel, ø6.216 x 0.059	6	13.0	78	
6	Complete Transition Piece		1		291.1	291.1
6.1	Transition Piece	Steel, ø6.6 x 12	1	291.1	291.1	
7	Fairleads		3		17.3	51.9
7.1	Fairlead		1	17.3	17.3	

Table 3.1: Part list for the original floating platform of the TetraSpar offshore floating support structure supplied by Stiesdal Offshore Technologies. The parts were up-scaled from the 1:60 model and adjusted from PVC to steel.

The mass of the model was taken during the measurement campaign. The recorded mass of the counter weight and the semi-sub are given with different configurations in Table 3.2. The mass, CoG, and CoB were calculated in the engineering design software, Genie and HydroD.

Table 3.2: Properties of the DTU 10 MW RWT, floating platform, and counter weight of the different designs.

Sub System	Mass (tonnes)	Inertia (Ixx) about COG (Mg*mˆ2)	Inertia (Izz) about COG (Mg*mˆ2)	COG (x,y,z) or z (m)
DTU 10 MW RWT	1240	1.90E6	6.06E6	(0.29,0,88.4)
Original Floating Platform	3570	3.04E6	3.88E6	-15.1
Alternative Floating Platform A	2810	2.39E6	3.05E6	-14.1
Alternative Floating Platform B	2810	3.04E6	3.88E6	-14.1
Original Counter Weight	8070	4.07E6	8.15E6	-80.4
Alternative Counter Weight A	5350	2.70E6	5.40E6	-100
Alternative Counter Weight B	5260	2.65E6	5.31E6	-128

Table 3.3: The total system properties of the original and alternative designs in the operational phase and transportation phase.

System	Mass (tonnes)	Inertia (Ixx) about MWL (Mg*mˆ2)	Inertia (Izz) about MWL (Mg*mˆ2)	COG (m)	COB (m)	Hydrostatic Heave Stiffness (N/m)	Hydrostatic Pitch Stiffness (N m/rad)
Operational Phase (Spar)							
Original Design	13170	7.28E7	1.25E7	-46.2	-25.4	9.23E5	2.70E9
Alternative Design A	9750	7.22E7	9.04E6	-49.6	-33.6	9.23E5	1.51E9
Alternative Design B	9761	1.06E8	9.94E6	-55.3	-38.3	9.23E5	2.46E9
Transportation and Installation Phase (Semi-Submersible)							
Original Design	4810	1.55E7	3.94E6	11.6	-4.2	9.04E6	3.04E9
Alternative Design A	4050	1.46E7	3.11E6	17.3	-7.8	7.07E6	3.47E8
Alternative Design B	4050	1.46E7	3.11E6	17.3	-7.8	7.07E6	3.47E8

3.4 Mooring and Suspension Line Properties

A typical catenary mooring system was used for the model tests [19]. A traditional three line mooring system was used that can be seen in Fig. 3.4 and 3.8. Due to the limitations of the wave basin the catenary model must be truncated. The dimensions of the scaled-up catenary mooring system is given in Table 3.4. The same chain size and material is used for the design of the mooring and counter weight suspension system, which are also listed in Tab. 3.4. The equation to calculate mooring material stiffness was taken from DNV [11]. A diagram showing the mooring configuration during the wave tank tests is given in Fig. 3.8. The configuration of the top-view of the floating support platform is also shown in addition to the mooring line configuration.

Table 3.4: Parameters of the model scale catenary mooring.

Anchor radius from platform centerline	600.0 m
Anchor Depth from platform centerline @ MSL	180 m
Fairlead radius from platform centerline	44.7 m
Fairlead depth from platform centerline	-30.3 m
Unstretched line length	604.8 m
Assumed wet mass per unit length	590 kg/m
Estimate of equivalent mooring system vertical mass	702 tonnes
Normal Chain Diameter	0.236 m
Material Equivalent Diameter	0.333 m
Material Cross Sectional Area	0.0875 m^2
Material Stifness	5.22E+10 N/m^2
Material Axial Stiffness	4.57E+09 N

3.5 Design Basis

3.5.1 Environmental Conditions

Environmental conditions, summarized by Li [24], were used as a design basis for the following study. The environmental conditions are representative of the Norwegian coast, for the site Norway 5. The conditions Norway 5 have similar water depth of 202 m compared the model of the TetraSpar at 180 m water depth. To perform a parametric design study the floating platform response is analyzed at rated wind speed during average wave conditions for that given wind speed. The environmental conditions are listed in Tab 3.5. Rated conditions were chosen for the study since the mean pitch offset at rated power was used as a design requirement. Operation at rated power is one of the design cases in [25] as it results in the maximum operational thrust force on the turbine. Operation at rated power was also considered to provide a representative estimate of fatigue conditions.

For the short term environmental wave statistics the JONSWAP wave spectrum [26] is used with a peakedness value of 3.3. Short term wind profiles are generated using TurbSim. Wind profile characteristics are investigated for a class 1 wind turbine with class C turbulence defined by the IEC 61400-3 offshore wind turbine standard [25]. The Kaimal wind spectrum is used with a power law exponent of 0.14 to account for wind shear.

Two current models are used in the design. A normal current model and an extreme current model is specified by DNV [25]. Due to the lack of current data it is assumed that the extreme 50 year current value is 1.2 m/s, the 1 year current value is 1.0 m/s, and the normal current is 0.25 m/s. A standard current power exponent of $\frac{1}{7}$ is used. The current profile can be defined using equation (3.1).

Table 3.5: Environmental Conditions.

Condition	NSS Rated	SSS Rated	NSS V_{out}	SSS V_{out}	Extreme H_{s1}	Extreme V_{hub1}	Extreme H_{s50}	Extreme V_{hub50}
V_{hub} (m/s)	11.4	11.4	25.0	25.0	38.5	40.4	40.0	42.9
H_s (m)	2.7	7.9	6.1	12.3	13.5	11.8	15.6	13.4
T_p (s)	11.1	11.8	11.3	12.9	13.1	11.6	14.5	13.1

Table 3.6: Design requirements of the TetraSpar floating support structure.

Design Requirement	
Mean Pitch Offset at Rated Power	5°
Maximum Pitch Offset	10° or θ_{crit}
Maximum Nacelle Acceleration	0.4 g
Line Tension	>0 N
Line Tension Safety Factor, k	5

$$V_c = V_c(0)(\frac{(z+d)}{d})^{\frac{1}{7}} \tag{3.1}$$

3.5.2 System Design Requirements

The general requirements for floating wind turbines will be used as a basis for the design. There are sub-requirements for the counter weight suspension system that will be discussed in the following section, however the main requirement is to avoid zero tension in any of the lines. The general requirements for FOWT involve nacelle acceleration, platform pitch angle, and rigid-body natural frequencies. The pitch and acceleration design requirements have been proposed by industry to be conservative estimates of the requirements of a floating system [27, 28]. All design requirements are listed in Tab. 3.6.

To ensure a factor of safety for avoiding zero tension a statistical method will be used. Tension leg platforms also have a requirement to maintain positive tension in all connecting lines. In a study of tension leg platforms Bachynski [29] proposes that, assuming line tension probability can be represented by a Gaussian distributed process, a failure criteria can be represented using Eqn. 3.2. The mean value of the line with the lowest tension must be k standard deviations away from zero. An initial design requirement of 5 was chosen for k.

$$mean(T_{Lmin}) - k \cdot STD(T_{Lmin}) > 0 \tag{3.2}$$

For the design of floating wind turbines the maximum allowed pitch angle is assumed to be 10° [27, 28]. It will be seen that the maximum allowed pitch angle can be lower than 10° due to the requirements of the counter weight suspension system. It will be show that, for the original design, at counter weight depth of 140 meters the critical pitch angle drops below 10°. For different support structure designs this depth can vary. Depending on the depth of the counter weight, the design criteria can be 10° set by the turbine operation or be below 10° and driven by support structure requirements. It should be noted that the requirement set by the critical pitch angle of the counter weight system is more critical as the risk involved with exceeding this angle has a greater consequence.

3.6 DTU 10MW Reference Wind Turbine

The DTU 10MW Reference Wind Turbine (RWT) has been developed by DTU and was upscaled from the NREL 5MW RWT [10]. The DTU RWT was developed to provide a basis for research and investigation of larger turbines. Floating wind energy makes installation of larger turbines possible through land based installation and tow out. Larger turbines have been identified as having the potential to decreased the levelized cost of energy (LCOE). Larger turbines have the potential to decrease LCOE due to having increased swept wind area, having access to increased wind speeds at higher elevations, and having a more favorable balance of system costs [30].

The main dimensions and properties of the DTU 10MW RWT are given in Tab. 3.7. The turbine is a conventional upwind turbine with clockwise rotation. The DTU 10 MW RWT is designed to handle IEC Class 1A winds, however the wind conditions investigated in this study are Class 1C as offshore turbulence is low [25].

Table 3.7: The parameters of the DTU 10 MW RWT.

Properties	DTU 10 MW RWT
Rated Power	10 MW
Hub Height	119 m
Rotor Diameter	178.3 m
Minimum Rotor Speed	6.0 rpm
Maximum Rotor Speed	9.6 rpm
Maximum Tip Speed	90 m/s
Cut In Wind Speed	4 m/s
Rated Wind Speed	11.4 m/s
Cut Out Wind Speed	25 m/s
Shat Tilt Angle	5°
Rotor Precone Angle	-2.5°
Gear Box Ratio	50

The DTU 10MW RWT has tower extending from 0 to 115.63 m above the mean water line (MWL). The TetraSpar has a transition piece that extends 16.5 m above the MWL.

To account for this overlap in height between 0 and 16.5 m, the fist 16.5 m of the DTU 10MW RWT tower was removed, this system will be referred to as the Modified DTU 10 MW RWT. Figure 3.7 shows a model illustration of the modified DTU 10 MW RWT with the bottom section of the tower removed to comply with the interface conditions of the TetraSpar support structure. Only the tower section was modified from the original DTU 10 MW RWT.

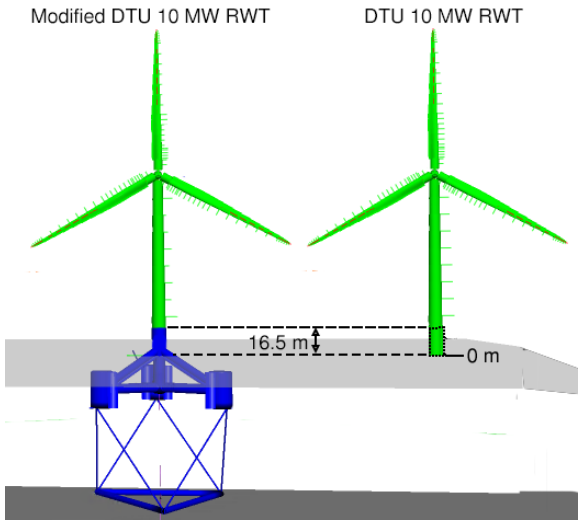

Figure 3.7: The DTU 10 MW RWT and the modified DTU 10 MW RWT with the bottom section of the tower removed to comply with the interface conditions of the TetraSpar support structure.

There are two different turbines used thought this report: the Modified DTU 10 MW RWT and the DTU 10 MW Test Turbine. The Test Turbine is used in the DTU DHI wave basin tests. More details about the Test Turbine and the differences between it and the DTU 10 MW RWT are given by Bredmose [31]. The properties of the DTU 10 MW Test Turbine are used to tune the numerical model's damping coefficients to match the physical 1:60 model. The properties of the Modified DTU 10 MW RWT are used for all numerical simulations, other than model tuning, presented in this report. The Modified DTU 10 MW RWT is used for the simulations as it better represents reality. The differences between the DTU 10 MW Test Turbine and the Modified Turbine are significant as seen by the large difference in inertia and mass presented in Tab. 3.8.

Table 3.8: Properties of the Modified DTU RWT and the DTU Test Turbine.

Properties	Modified DTU 10 MW RWT		DTU 10 MW Test Turbine (scaled up)	
	Mass (tonnes)	Ixx about the MWL (kg m^2)	Mass (tonnes)	Ixx about the MWL (kg m^2)
Tower	574	2.13E+06	427.7	2.28E+06
Nacelle	446	6.22E+06	787.6	1.10E+07
Hub	105.5	1.49E+06	105.5	1.52E+06
Three Blades	117.3	1.76E+06	114.3	1.87E+06
Total	1242.8	1.16E+07	1435	1.67E+07

3.7 TetraSpar DTU DHI Model Scale Tests

The DTU DHI Model scale tests of the TetraSpar [23] were used to calibrate the numerical model. The goal of the calibration was to match the damping coefficients extracted from the model scale tests [19]. Linear and quadratic damping coefficients were taken from these tests. The test set up is shown in Fig. 3.8.

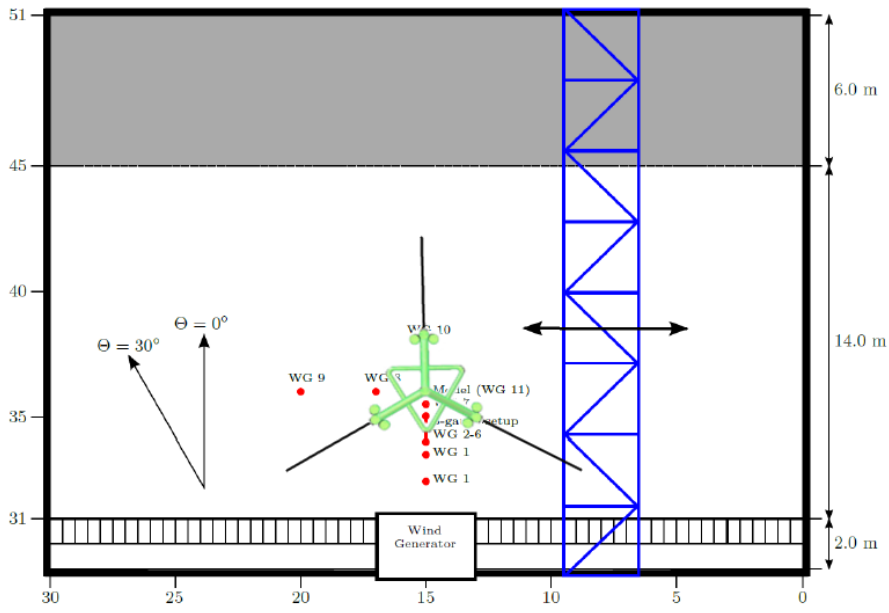

Figure 3.8: Wave tank test set up for the TetraSpar Model tests at DHI. The TestraSpar floater and counter weight are shown to depict the model configuration relative to wave and wind direction.

In addition to calibrating the motion data of the floating platform, other physical measurements were qualitatively analyzed to ensure that numerical model made physical sense. The following instrumentation was used to collect acceleration, line tension, and motion:

- Two 6 DOF Qualisys MotionTrack displacement measurement systems at the floater center and nacelle
- Two 6 DOF acceleration at the floater center and nacelle
- Two 3 DOF accelerations at the floater tanks
- Three counter weight (keel) gauges
- Three mooring gauges

Chapter 4

Design and Analysis of the Counter Weight Suspension System

4.1 Counter Weight Description and Design Requirements

The suspended counter weight of the TetraSpar is a unique design feature invented by Stiesdal Offshore Technologies A/S [18]. The purpose of the suspended mass is to provide stability to the structure to resist overturning moments from wind and waves. The counter weight is suspended using six suspension lines. It will be shown that the two bodies behave as a rigid body as long as there is positive tension in all suspension lines. The limit to which the floating platform can pitch and still maintain positive tension is identified analytically by solving for equilibrium of moments and forces in six degrees-of-freedom (DOF).

The counter weight's draft and mass can be adjusted to optimize the structural and hydrodynamic properties of the floating system. In this regard the counter weight is a useful design tool which can be used to tune system properties without significant structural design changes. An increase in draft or mass of the counter weight increases the hydrostatic stiffness in pitch, and therefore can reduce mean pitch angles. However, this change in stiffness can also alter the dynamic behavior of the floating system in a dynamic wind and wave environment.

The goal of the parametric study is to decrease the mass of the system. An understanding of the counter weight suspension system is necessary to understand the limit to which the counter weight's mass can be decreased. There are two requirements for the counter weight suspension system (1) none of the lines shall have a zero or negative tension and (2) the pitch angle shall not exceed the geometrical limit that would allow for the suspension lines to pivot about the fairlead. In a physical system the critical pitch angle will always be related to (1), the chain tension limit, since the pitch angle resulting in zero tension in one of the lines occurs before the geometric limit.

4.2 Providing Hydrostatic Stability

The large mass of the counter weight, seen in Fig. 3.1, lowers the center of gravity of the structure and provides a restoring moment for the structure in pitch. It is important to minimize the average pitch of the turbine to provide the turbine with standard horizontal wind conditions, this will maximize power production and avoid excessive vertical velocities seen by the blades.

The formula for hydrostatic pitch stiffness is given in Eqn. (4.1) [12]. Since the water plane area is small for the design in the spar configuration, this term results in a negligible contribution to the stiffness. The stiffness equation can be written as Eqn. (4.2) to demonstrate the separate contributions to the hydrostatic stiffness from each body. Fig. 4.2 shows how the component of the weight acting in the x direction provides a restoring moment. Increasing the counter weight draft directly increases the moment arm and stiffness of the system in pitch. To benefit from the design's ability to extend the moment arm of the gravitational restoring force, it is possible to decrease the mass of the counter weight while maintaining the same stability properties. Also, a larger counter weight draft results in a larger system pitch inertia, which is expected to reduce dynamic pitch motions resulting from dynamic environmental loading.

$$C_{55} = \rho g V(CB - CG) + \rho g \iint_{A_{WP}} x^2 ds \tag{4.1}$$

$$C_{55} = B_P CB_P - W_P CG_P + (B_{CW} - W_{CW}) CG_{CW} - W_T CG_T \tag{4.2}$$

In Eqns. (4.1) and (4.2) the following variables are used to represent the physical parameters: C_{55} the hydrostatic pitch stiffness, A_{WP} the area of the water plane, B the buoyancy force, W the gravitational force, CB the center of buoyancy, and CG the center of gravity. The subscripts T, P, and CW, respectively represent each body: the turbine/tower, the floating platform, and the counter weight.

4.3 Suspension System Line Tension

The hanging counter weight design utilizes chains to transfer axial forces in a truss configuration. It is necessary to prohibit zero tension in the suspension system to avoid relative motion between the two bodies and to prevent snap loads in the suspension system. When the floating platform is in it's undisturbed state there is a pre-tension in all of the lines due to the gravitational force of the counter weight balancing the buoyancy force of the floating platform. When the body displaces in pitch the forces in these suspension lines change to transfer the restoring moment provided by the counter weight. An analytic solution to the tension in the suspension lines is presented. Then, the geometric pitch limit that results in

zero tension is identified. This geometric pitch limit is dependant geometric angles of the structure and on the angle of attack of the environmental force, α.

4.3.1 Six Degree-of-Freedom Solution

Equations (4.6) through (4.9) describe the static equilibrium of forces and moments on the counter weight experienced during a pitch offset. Figure 4.2 shows the combination of vertical forces and horizontal forces that would be transferred from the counter weight through the suspension lines. The equations for the analytic solution depend mostly on the geometric angles that the suspension lines make between the floating platform and the counter weight.

The solution to the static tension equations are formulated using several geometric and environmental angles. These angles are depicted in Fig. 4.1. The minimum geometric angle between the horizontal x-y plane and the counter weight suspension line is given by ϑ, this angle is used to transform the line tensions into their horizontal and vertical components. The angle ϑ is the same for all of the suspension lines. The net angle of attack of environmental forces is given by α, this angle can be changed to determine how tension varies when the structure rotates in different directions. The angle, Ψ_n, represents the angle in the x-y plane that the counter weight suspension Line n, makes with the global x axis, with n being the number of the suspension line. Figure 4.1 shows the angle, Ψ_6, that Line 6 makes with the x axis in the x-y plane. The term $cos(30)$ is used in Eqn. (4.9) to account for the angle that the tension moment arm makes with a line extending from the center of the counter weight to the fairlead. This cosine term can change for different system configurations.

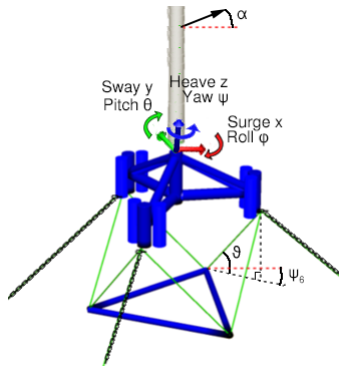

Figure 4.1: Illustration of the angle variables in the counter weight suspension system.

$$\sum F_z = W_Z, \qquad \sum F_x = W_X \tag{4.3}$$

$$\sum F_X = \frac{cos(\vartheta)}{cos(\alpha)}[cos(\psi_1)T_1 + cos(\psi_2)T_2 + cos(\psi_3)T_3 + cos(\psi_4)T_4 + cos(\psi_5)T_5 + cos(\psi_6)T_6] = W_X \tag{4.4}$$

$$\sum F_Y = \frac{cos(\vartheta)}{sin(\alpha)}[sin(\psi_1)T_1 + sin(\psi_2)T_2 + sin(\psi_3)T_3 + sin(\psi_4)T_4 + sin(\psi_5)T_5 + sin(\psi_6)T_6] = W_Y \tag{4.5}$$

$$\sum F_Z = sin(\vartheta)[T_1 + T_2 + T_3 + T_4 + T_5 + T_6] = W_Z \tag{4.6}$$

$$\sum M_X = sin(\vartheta)[T_1 + T_2 - T_5 - T_6] = 0 \tag{4.7}$$

$$\sum M_Y = sin(\vartheta)[-\frac{1}{2}(T_1 + T_2 + T_3 + T_4) + (T_3 + T_4)] = 0 \tag{4.8}$$

$$\sum M_Z = -cos(\vartheta)CW_X[cos(30)T_1 - cos(30)T_2 + cos(30)T_3 - cos(30)T_4 + cos(30)T_5 - cos(30)T_6] = 0 \tag{4.9}$$

4.3.2 Static Limit of Pitch in One Direction

Figure 4.3 demonstrates the behavior of the chain tensions as the structure pitches in response to environmental loading, illustrated in Fig. 4.2. When the floating system is in the undisturbed position with zero pitch, the tensions in all of the lines are positive and equal. As environmental forces create overturning moments, the structure rotates in pitch until equilibrium is obtained with the structure's hydrostatic pitch restoring moment. To transfer the restoring moment through the suspension chains, the tension in Line 2 increases and the tension in Line 1 decreases to maintain moment equilibrium as seen in Fig. 4.3. The limit to the system's range of motion in pitch is experienced when the tension in Line 1 decreases to zero. As the lines are made out of chain or synthetic rope they cannot transfer compressive forces or bending moments. For the original design with the counter weight located at 80 m water depth, the critical pitch angle is found to be 24.2° when the pitch axis is aligned with 90°.

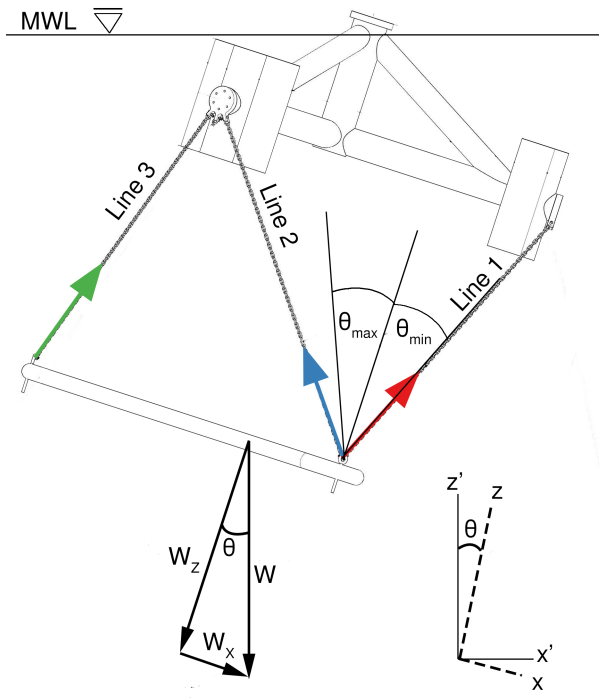

Figure 4.2: Analytic chain tension for a pitch direction of 90° as defined in Fig. 3.3.

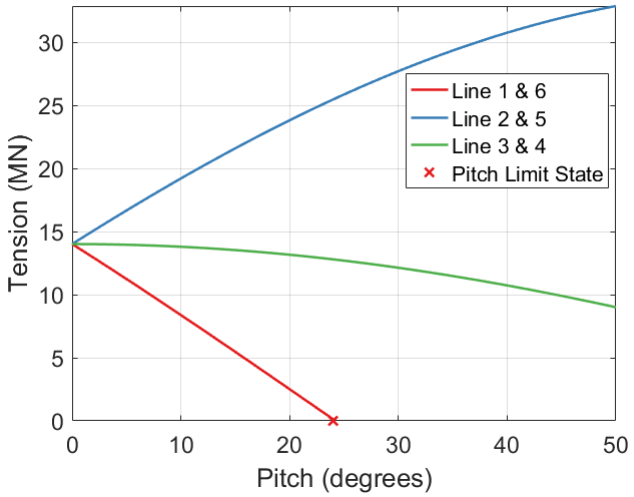

Figure 4.3: Static chain tension for different angles of pitch as illustrated in Fig. 4.2.

To determine if the critical pitch angle is a function of the geometry or both the geometry and the weight two separate mass were investigated for the counter weight. Figure 4.4 shows the analytic solution of line tension for two separate counter weight configurations. In these configurations the only change is to the mass of the counter weight. Counter weight masses of 8,000 tonnes and 12,000 tonnes are investigated. The pre-tension increases for the system with an increased mass, however the pitch limit state remains the same regardless of mass. In Figure 4.4 the line tension in Line 1 & 6 intersect with the zero line tension at the same angle of pitch of 24.2 degrees. This demonstrates that the pitch limit is governed by the geometry of the system and not significantly influenced by the mass. Although the pitch limit does not change for the two systems, the system with a larger counter weight mass will have increased stiffness and as a result be less likely to exceed the pitch limit.

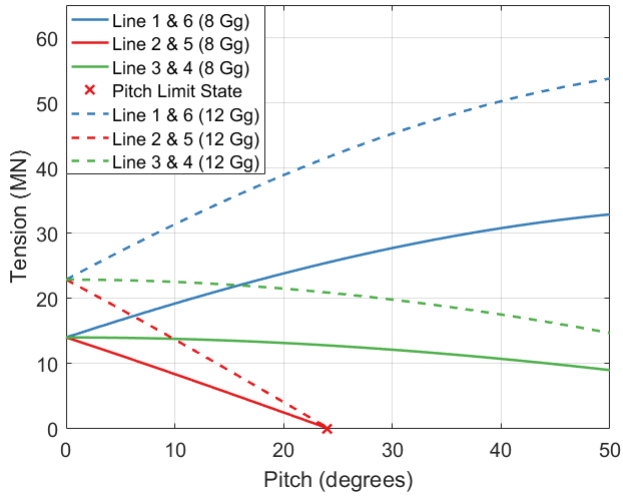

Figure 4.4: Static chain tension for different angles of pitch and for two separate mass of the counter weight as illustrated in Fig. 4.2.

4.3.3 Static Limit of Heel in Any Direction

The allowable rotation angle changes for rotation about different axes. To simplify the analysis, heel is defined as the angular rotation about an axis lying on the x-y plane. In this way roll and pitch in the global coordinate system are combined and represented with one angle, heel in the local coordinate system. This local-heel will be referred to in this paper. Fig. 3.3 shows the global axis with the heel axis aligned with 90° for heel about the y' axis, referred to as heel about 90°. Heel about 90° is caused by the net environmental forcing angle, α, of 0°. By identifying the critical heel angle of Fig. 4.3 for heel about any axis, the limiting critical heel angle is found. Fig. 4.5 shows the critical angle for heel about different axis. The critical angle is found to be equal and minimum for heel about 0, 60, 120, 180, 240, and 300°. The critical heel angle of the original design is 21.1°.

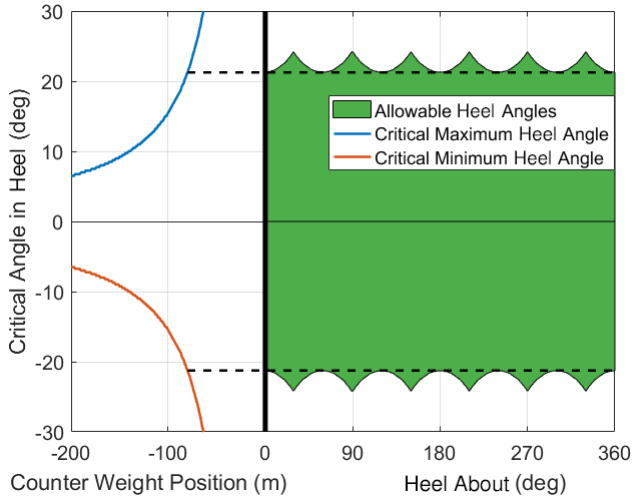

Figure 4.5: Critical platform heel angles for counter weight depth (left). The allowable heel angle for heel about an axis aligned with the degree convention from Fig. 3.3 for the original design at 80 m water depth (right).

This static analysis allows for the critical direction of heel to be identified. It also provides an estimate of the critical heel angle of the system. However, dynamic motions will introduce additional variability into the chain tension values. To investigate the dynamic behavior of the system, the maximum and minimum tensions in the suspension chains will be analyzed in the parametric optimization. In addition to considering the maximum and minimum chain tensions, cyclic tensions are analyzed to give an indication of each design's expected fatigue performance.

4.3.4 Static Limit of Pitch Dependant on Depth

To demonstrate the behavior of the chain tension for decreasing counter weight depth the chain tension in three of the suspension lines is plotted for changing counter weight depth in Fig. 4.6. To analyze the behavior of the chain tension, the analytic static tension solution is given for an extreme environmental wind moment. Wave moments are not considered in the static solution. This environmental wind moment will cause the systems to pitch depending on the hydrostatic restoring force of that system. Systems with larger counter weight depths will have greater hydrostatic pitch stiffness and pitch less.

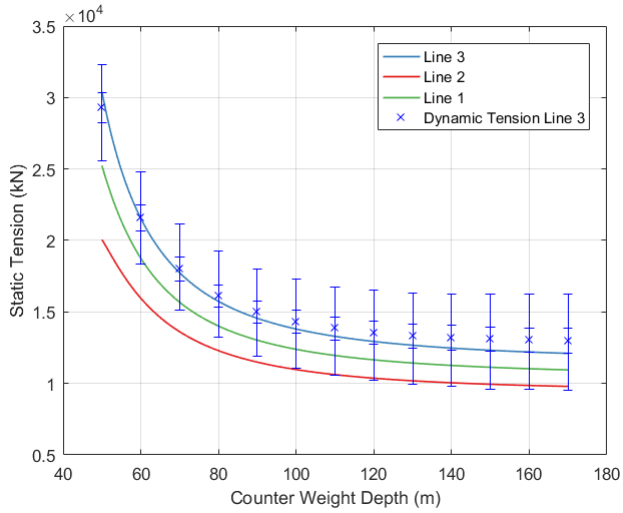

Figure 4.6: Analytic chain tension for a fixed counter weight mass and changing counter weight depth along with numerical results.

It can be seen that for increasing counter weight depth the chain tension in all of the lines decreases. This is caused mostly by the decrease in the angle that the suspension chains make with the vertical axis of the floating platform. This decrease in angle makes it easier to transmit vertical forces. This decrease is also caused by the decrease in pitch angle required to achieve the same restoring moment.

The static analytic solution is given for the solid lines in Fig. 4.6. To know the limit to which the counter weight can be lowered, the dynamic range of line tensions must be known. A dynamic time domain numerical model is built and discussed in the parametric study. In Fig. 4.6, results from the numerical model are given to demonstrate how the line tensions vary dynamically for operation under rated-average conditions. The results are based off of single one hour time domain simulations. These dynamic results, given for line 3, also used to validate the analytic static solution. The range of the dynamic line tensions is greatest at small and large depths. The dynamic range is smaller at medium depths of 100 m, but these deviations in range are not greater than 20% of the smallest range observed. The dynamic range is expected to increase when considering more extreme environmental conditions.

4.4 Rigid Body Behavior

As long as positive tension is maintained in all six chains, then the counter weight will behave as a rigid body and not pivot about the fairlead. This rigid behavior is a result of the six lines constraining the counter weight in all six degrees-of-freedom. For the counter

weight to move relative to the body would require deformation of the suspension lines. As the chains do not transfer bending moments, the only possible deformation is through axial elongation. This axial elongation through strain of the material results in small relative motion if: the suspension line stiffness is large and the suspension system natural frequencies avoid the natural frequencies of any environmental or operational forces. For the original design and the alternative designs selected, the relative motion, from where the body would be located statically, was found to be vary less than 1.5 m during all dynamic simulations.

To elaborate on the claim of rigidity, when there is positive tension in all lines it means that, physically, the counter weight is always ”pulling down” on the floating platform and the floating platform is always ”pulling up” on the counter weight. The bodies are trying to move in opposite directions, but cannot move further apart without axial elongation of the suspension lines. In this manner the counter weight system's design requirements are similar to a tension leg platform. However, unlike a tension leg platform, the counter weight is free to move with the floating platform and as a result is better designed to avoid zero tension.

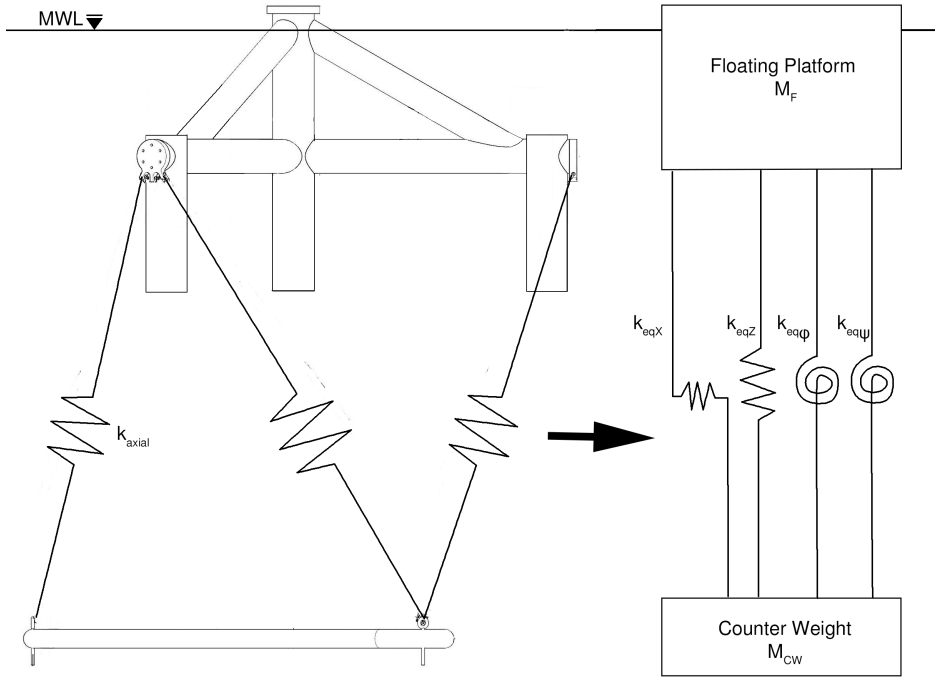

Figure 4.7: Multibody system with equivalent spring stiffness used to represent the axial stiffness provided by the six suspension lines. The floating platform has both stiffness from mooring and hydrostatic.

4.5 Multi-Body Behavior

The rigid body assumption must be checked by analyzing the stiffness and expected motion response of the muti-body system. To check the deformation and natural frequencies of the system, first the equivalent stiffness of the suspension system must be determined. This multibody system is shown in Fig. 4.7.

The two-body system in total has 12 DOF. The physical system is difficult to model analytically because of the non-linearity in the equivalent spring system. If the suspension lines were infinitely stiff, then the system would behave as a double pendulum. However, it is of interest to model the stiffness of the suspension system to determine the validity of such an assumption. Jankowski [32] gives the solution for a double pendulum system with the two-mass system connections represented with vertical springs. In the following analysis vertical springs represent the vertical equivalent stiffness of the suspension system. Using only vertical springs ignores pitch stiffness. The gravitational force responsible for the pitch stiffness of the counter weight introduces non-linearity into the system. To avoid this complex analysis it was decided to break the system into separate simplifications to approximate the natural frequencies of the system. First, the un-coupled 2 DOF stiffness in heave and yaw are analyzed since these DOF have little coupling with other DOF; see the un-coupled equation of motion in Eqn 4.10. This un-coupled system avoids the analysis of the double pendulum. From the the heave and yaw DOF it will be determined to what extent the suspension system influences the behavior of the total floating system in the subsequent hydrostaic analysis.

$$\begin{aligned} \ddot{X}\begin{bmatrix} M_{ii,F} & 0 \\ 0 & M_{ii,CW} \end{bmatrix} + \dot{X}\begin{bmatrix} B_{ii,F} & 0 \\ 0 & B_{ii,CW} \end{bmatrix} \\ +X\begin{bmatrix} K_{ii,Hyd}+K_{ii,Sus} & -K_{ii,Sus} \\ -K_{ii,Sus} & K_{ii,Sus} \end{bmatrix} = \begin{bmatrix} F_{ii,F} & 0 \\ 0 & F_{ii,CW} \end{bmatrix} \end{aligned} \tag{4.10}$$

Equation (4.10) shows the uncoupled equation of motion for the two-body system. The variables M, B, K, and F represent the respective mass, damping, stiffness, and force excitation of each DOF, ii. The sub-scripts F, CW, Hyd, and Sus, respectively represent the floating support structure, counter weight, hydrodynamic stiffness, and suspension system line stiffness.

4.5.1 Suspension System Equivalent Stiffness

The relative motion or vibration of the counter weight system is cause by a stiffness in the suspension chains. Following Eqns. (4.6)-(4.9), the counter weight suspension system equivalent stiffness can be calculated for each DOF. The equivalent stiffness in each DOF, described by Eqns. (4.11)-(4.16), are a function of the geometry and the axial stiffness of the suspension lines.

During environmental forcing the geometry of the lines will change and as a result of displacement from equilibrium. Constant material stiffness is assumed for the axial stiffness of the line. The values of stiffness to be used in subsequent analysis are linearized and derived from the geometry with zero initial displacement. The linearization is valid for small relative displacement between the counter weight and floating platform.

$$k_{eqX} = cos(\vartheta)[cos(\psi_1) + cos(\psi_2) + cos(\psi_3) + cos(\psi_4) + cos(\psi_5) + cos(\psi_6)]k_{axial} \tag{4.11}$$

$$k_{eqY} = cos(\vartheta)[sin(\psi_1) + sin(\psi_2) + sin(\psi_3) + sin(\psi_4) + sin(\psi_5) + sin(\psi_6)]k_{axial} \tag{4.12}$$

$$k_{eqZ} = 6sin(\vartheta)k_{axial} \tag{4.13}$$

$$k_{eq\phi} = cos(\vartheta)CW_X cos(30)4k_{axial} \tag{4.14}$$

$$k_{eq\theta} = cos(\vartheta)[4\frac{CW_X}{2} + 2CW_X]k_{axial} \tag{4.15}$$

$$k_{eq\psi} = cos(\vartheta)CW_X[6cos(30)]k_{axial} \tag{4.16}$$

Chapter 5

Hydrostatic and Frequency Domain Analysis

5.1 Hydrostatic Design

5.1.1 Installation Procedure

The original TetraSpar design consisted of separate phases for installation and operation. The original installation process uses the semi-submersible floating platform to provide stability during the transportation and installation phase. This design constraint of installation stability can result in an increased mass. To quantify the additional mass, that is required to meet the installation-stability requirements, alternative-lighter designs are proposed that require temporary stability or alternative installation methods.

Considering an installation procedure, that is similar to a conventional spar, will separate the added benefit of the counter weight technology from the two phase installation procedure. One of the main advantages of the TetraSpar is the ability to have a low draft during installation due to the hydrostatic stability of the semi-submersible floating platform. If it is not required to have two separate installation phases, the TetraSpar can be installed in the similar procedure to the Hywind spar [2]. During this installation procedure the turbine can be installed onto the floating support structure in the water. Since this installation procedure does not require the floating platform to act as a semi-submersible support structure, the greatest decreases in system mass can be achieved. It is the alternative Designs I & II presented in the parametric study that would require this installation procedure. This procedure can use a large offshore crane to perform the mating process between the floating support structure and turbine. The major downside of this installation method is that it would be expensive and large offshore crane resources would be limited. In addition to being expensive, the mating procedure between the floating support structure and turbine can be significantly limited by environmental conditions and available installation sites.

Moving towards a decreased in installation complexity and an increase in support structure weight, a support structure can be designed that follows the original installation procedure. This support structure must be stable and have a positive metacentric height when the turbine is attached to the upper floating platform. There are several ways to achieve this stability: buoyancy members can be included in the permanent design of the support structure, temporary buoyancy members can be installed for use during the installation phase, or additional stability can be provided using installation vessels. In the original design, the floating platform uses permanent buoyancy tanks to provide a large stability which allows for transportation and installation to the site of operation. This stability is large and would allow for transportation in a range of environmental conditions. Acceptable environmental conditions for installation can be identified as those that do not result in exceeding the critical heeling angle, for which after the structure has negative stability. The maximum heeling moment can also be identified as the maximum moment that the structure is able to counteract.

Designs A and B represent a structure with a small critical heeling angle and critical heeling moment. These designs would be limited to installation in mild environmental conditions. The original design has a large critical heeling angle and large critical heeling moment and could be installed in a large range of environmental conditions. A structural design that falls in-between the original design and the alternative Designs A & B is likely to be optimal. A design should be selected that provides a balance between the range of installation weather windows and weight of the support structure. The selected design would be driven by the selected limiting environmental conditions in which the semi-submersible structure is able to initiate installation. Installation procedures are not the focus of this report, but the metracentric height and righting moment curves are provided to demonstrate the floating platform design limitations and requirements.

5.2 Hydrostatic Stiffness

As discussed in the hydrostatic theory section, spar structures receive hydrostatic stiffness from the difference between the center of gravity and center of buoyancy, while semi-submersibles achieve a hydrostatic stiffness provided by their water plane area. It is a simple procedure to change the hydrostatic stiffness of the spar structure, this only requires changing the position or mass of the counter weight.

Sufficient hydrostatic stiffness is required to meet the installation requirements. Hydrostatic stiffness requriements can be defined by following the DNVGL-ST-N001 standard [33]. This standard states that ”the intact range of stability, about any horizontal axis, defined as the range between 0° inclination and the smallest angle at which the righting arm (GZ) becomes negative shall not be less than the value specified.” A visualization of this requirement is provided in Fig. 5.1, where the dynamic angle represents the stability angle. The defined dynamic angle must be less than the 2nd intercept angle. The wind overturning arm will be estimated by assuming an initial wind overturning moment of 248 MN-m that decreases with increasing inclination angle since the rotated tower will experience a

decrease in drag due to the relative change in angle of attack of the wind.

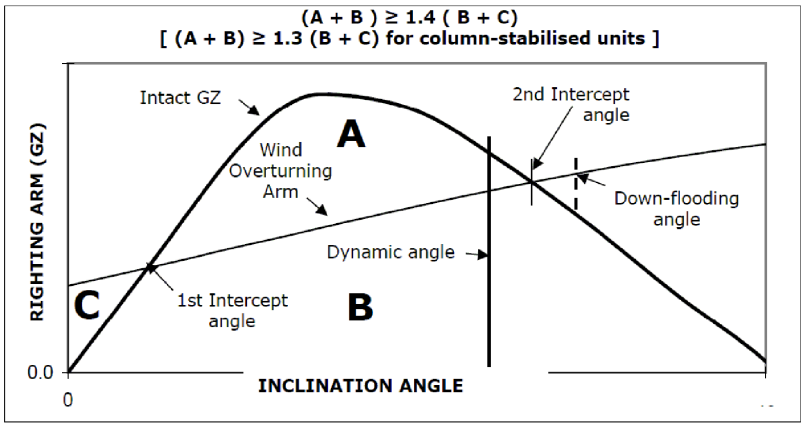

Figure 5.1: The stability requirement of a mobile offshore unit (MOU) or semi-submersible.

Changing the hydrostatic stiffness of the semi-submersible platform is a complex procedure. In addition to being difficult to change, it is also difficult to identify the design requirements of the semi-submersible structure. The spar configuration has design requirements being related to the operation of the wind turbine and constraints of the suspension system. The main goal of the semi-submersible system should be to provided the turbine with sufficient stability during the transportation and installation phase. Since the semi-submersible configuration is only used during transportation and installation, the environmental conditions in which installation is allowed to take place can be restricted. Restricting the environmental conditions, in which installation can take place, lightens the hydrostatic requirements and enables a lighter semi-submersible structure design.

Since the water plane area is small for the design in the spar configuration, this term results in a negligible contribution to the stiffness. The stiffness equation can be written as Eqn. (4.2) to demonstrate the separate contributions to the hydrostatic stiffness from each body. Fig. 4.2 shows how the component of the weight acting in the x' direction provides a restoring moment. Increasing the counter weight draft directly increases the moment arm and stiffness of the system in pitch. To benefit from the design's ability to extend the moment arm of gravitational restoring force, it is possible to decrease the mass of the counter weight while maintaining the same stability properties. Also, a larger counter weight draft results in a larger system pitch inertia, which will reduce dynamic pitch motions resulting from dynamic environmental loading.

5.3 GM and GZ Curves

The metacentric height and moment curves give a description of hydrostatic stability for different degrees of pitch. Semi-submersible structures have nonlinear hydrostatic stiff-

ness for varying degrees of pitch. As a result it is necessary to look at these metacentric height and moment curves to determine the range of stability of the structure for when the metacentric height becomes negative. These curves are also important to identify the maximum supplied restoring moment. These GM and metacentric height curves are shown for the structure's operational phase and installation phase.

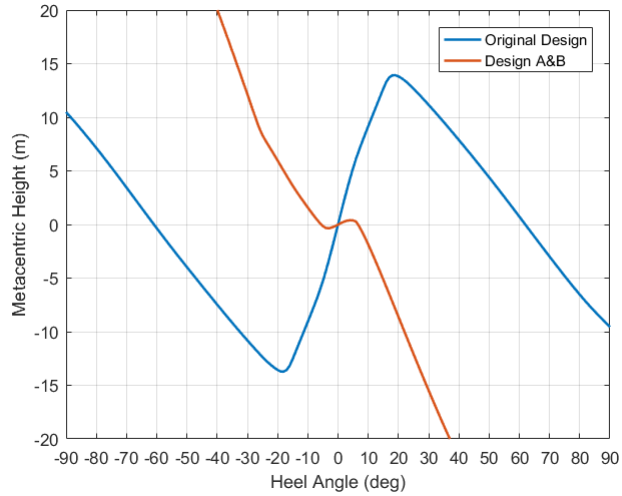

Figure 5.2: The metacentric height for different angles of heel for the TetraSpar in the transportation configuration.

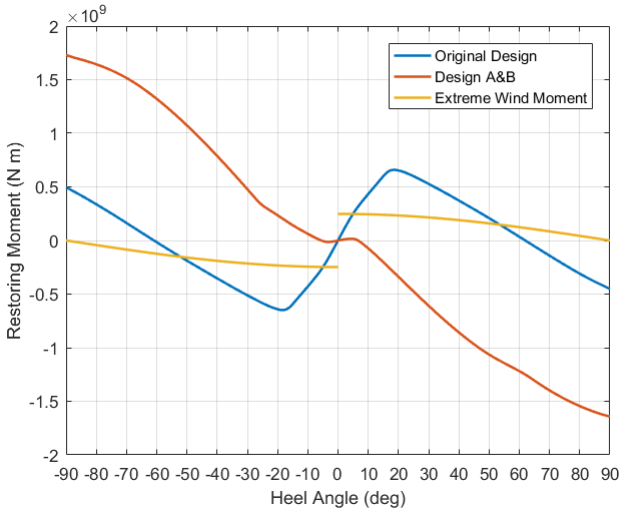

Figure 5.3: The restoring moment for different angles of heel for the TetraSpar in the transportation configuration.

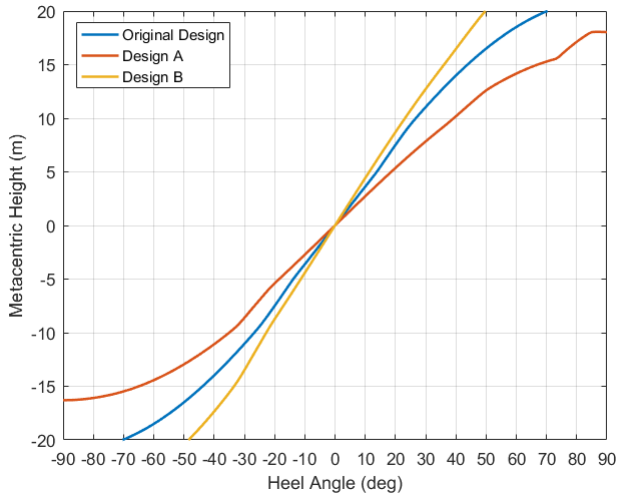

Figure 5.4: The metacentric height for different angles of heel for the TetraSpar in the operation configuration.

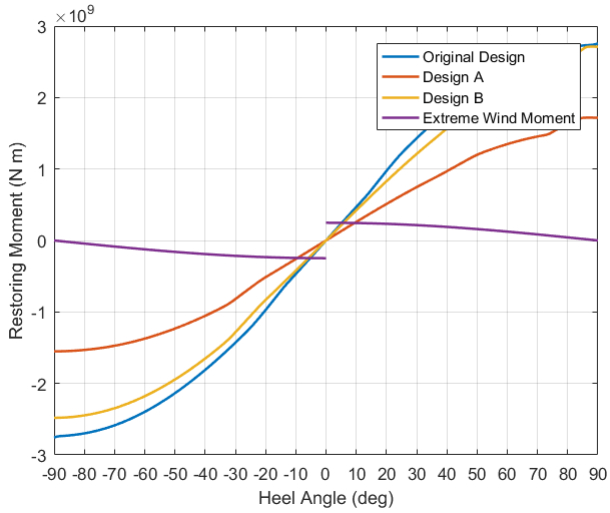

Figure 5.5: The restoring moment for different angles of heel for the TetraSpar in the operation configuration.

It can be seen from Fig. 5.3 that the restoring moment provided by the alternative designs A&B do not meet the DNVGL design requirements. The original design meets the DNVGL design requirements from Fig. 5.1; it is assumed that a down-flooding angle does not exist for a floating wind turbine or that it occurs only at very extreme angles greater than 60°. It can be seen from Fig. 5.5 that the restoring moment provided by all

of the designs in the operational phase is sufficient to meet the DNVGL requirements for stability.

5.4 Added mass and Potential Damping

When calculating the added mass and potential damping in the frequency-domain it is assumed that the two bodies, connected with suspension lines, behave as a rigid body. Once the added mass is known, this rigid-body assumption will be checked.

The added mass and potential damping is assumed to be a function of frequency. Using potential flow theory, the added mass and potential damping, of the original and alternative Designs A & B, are calculated for frequencies between 0 and 2π radians. Figure 5.6 separates the added mass of the original design into the contributions from the upper floating platform and the counter weight. The upper floating platform has an increased draft during operation compared to transportation, resulting in different hydrostatic properties. The different added masses for both transportation and operation are also shown for the original design. Figure 5.7 shows the potential damping and also separates the different components for the original design.

The three designs that have been analyzed in the frequency domain, the original and alternative Designs A & B, show how changing the structural design also changes the induced added mass and potential damping. Figure 5.6 shows the separate designs in the transportation phase and the operational phase for the original design.

The transportation configuration of Designs A & B are the same since the transportation phase does not include the counter weight. Also, since the only difference between Designs A & B is the depth of the counter weight, they have the same added mass and potential damping in heave, surge, sway, and yaw. The only difference in added mass or potential flow between Designs A & B is the pitch and roll degrees of freedom. This is expected and can be calculated analytically by considering the moment arm of the counter weight.

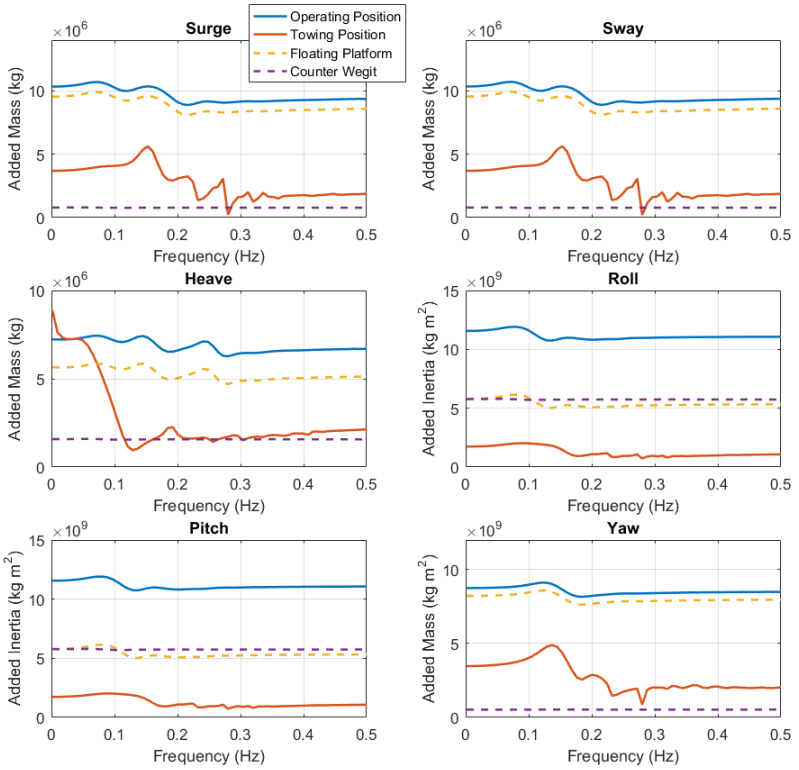

Figure 5.6: The added mass of the original design. The separate contributions from the two bodies in the operational phase are shown and the transportation phase is also included.

The added mass in all degrees of freedom have an added mass at zero frequency and at infinite frequency. The variation in added mass across the analyzed frequencies is the largest for the floating platform in the towing position. This variation in added mass is especially large for the heave degree-of-freedom.

Comparing the added mass and inertia of the original design in the operational position identifies in which DOF the added mass significantly effects the total system properties. The added mass and inertia in surge, sway, heave, and yaw all add over 50% of the mass or inertia to the system. The added mass in pitch and roll does not have as large of an effect changing the system properties. The values of original design's surge and heave added mass at zero frequency are 10,300 tonnes and 7,200 tonnes, these values are significant in comparison with the mass of the system of 13,300 tonnes. Comparing the pitch added inertia to the inertia shows that the pitch added inertia contributes a smaller percentage of the total inertia. The Original Design's pitch inertia is 7.28E10 kgm^2 compared to the added pitch inertia at zero frequency of 1.16E10 kgm^2. The Original Design's yaw inertia 1.25E10 kgm^2 compared to the added yaw inertia at zero frequency of 8.75E9 kgm^2.

The contributions of the counter weight are separated in Fig. 5.6. Separating the added mass of the counter weight from the floating platform shows that the counter weight added mass effects the pitch and roll DOF the most, but also has an effect on the heave added mass. The added mass of the counter weight is constant and shows little variation with frequency for all DOF; this verifies that that constant added mass coefficients can be used to represent the added mass of the counter weight. The added mass shows convergence to the value of added mass at infinite frequency at 1 Hz for all of the designs, seen in Fig. 5.7.

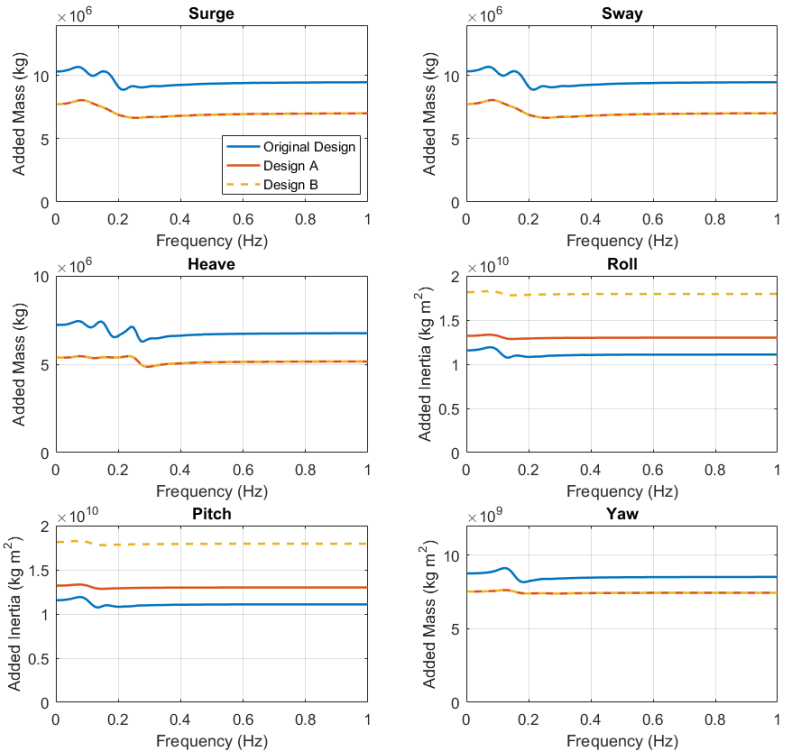

Figure 5.7: The added mass and inertia of the three designs: the original design, Design A, and Design B.

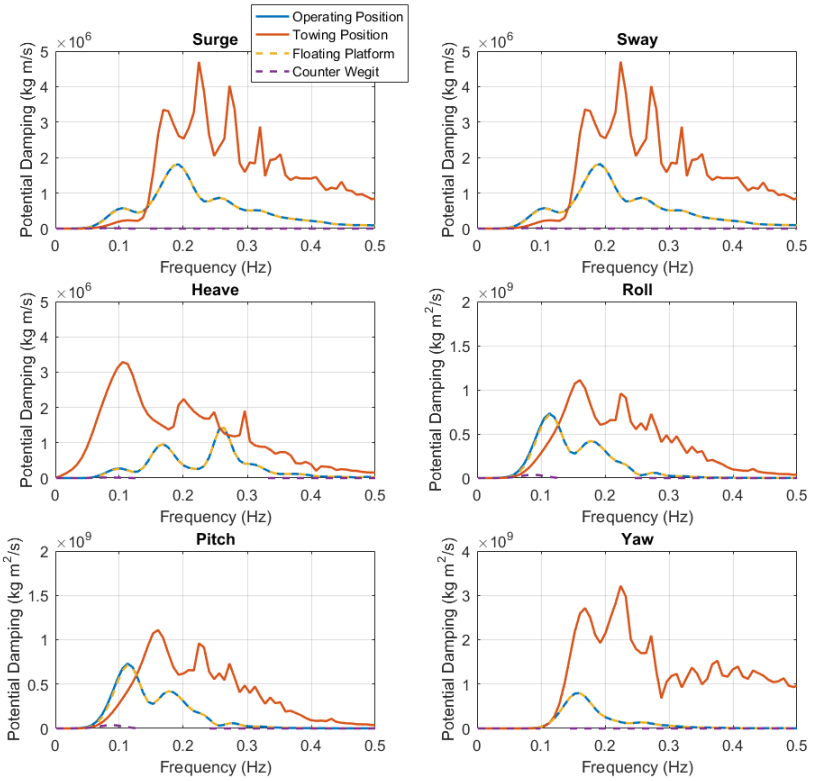

Figure 5.8: The potential damping of the original design. The separate contributions from the two bodies in the operational phase are shown and the transportation phase is also included.

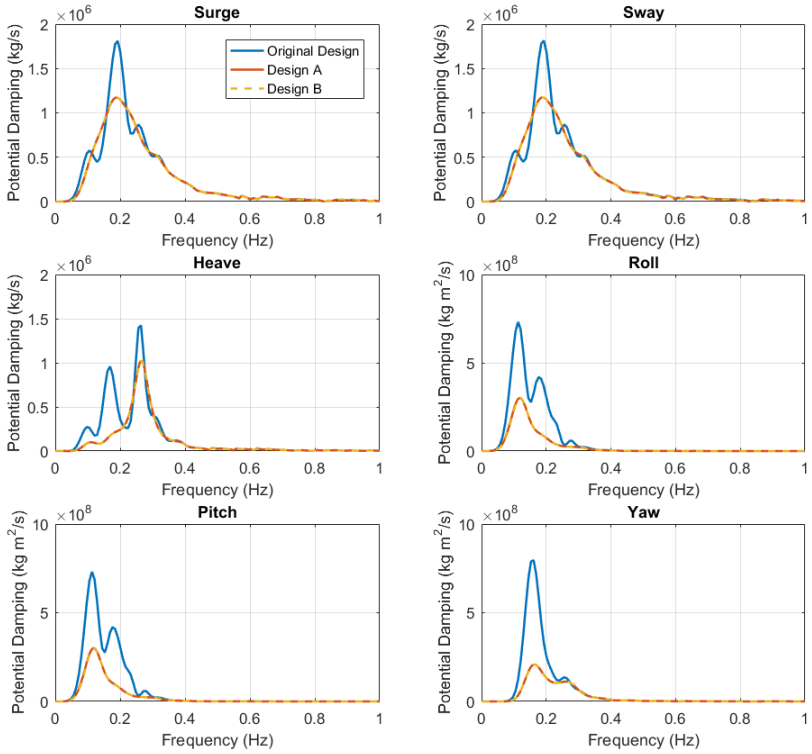

Figure 5.9: The potential damping of the three designs: the original design, Design A, and Design B.

5.5 Multi-Body Vs. Single-Body

Physically the TetraSpar consists of two bodies connected by chains. The system can be modeled as a rigid-body or a two-body system. The stiffness of the connection lines will determine if the system can be assumed to behave as a one or two-body system. Figure 5.10 shows the 12 DOF system.

The two bodies can be connected using chains or synthetic rope. The stiffness of the chain system will be investigated to determine if the stiffness of the chains influences the behavior of the hydrostatic/hydrodynamic system. To determine if the system can be assumed to be a rigid body the influence of chain stiffness will be analyzed in each degree of freedom separately. For the heave and yaw DOF, coupling with these DOF and other DOF is low and can be analyzed independently. The pitch and roll DOF are influenced by the heave DOF and these two motions are coupled when both heave and pitch are excited.

5.6 System Stiffness

The procedure for calculating the hydrostatic, mooring, and suspension system stiffness have given in previous chapters. Here the multi-body system stiffness will be analyzed to determine if the stiffness of the multi-body system effects the rigid body natural frequency. The multi-body analytical solution for the system in pitch and roll is difficult to obtain since these degrees-of-freedom result in displacement of the counter weight in surge, sway, and heave and are coupled. The un-coupled equation of motion is given in Eqn. 4.10.

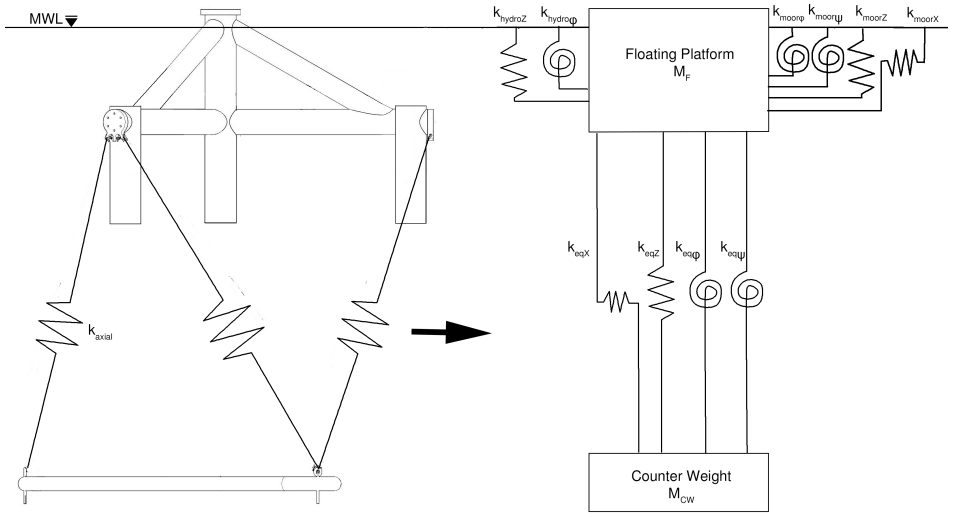

Figure 5.10: The stiffness of the suspension system, hydrostatic, and mooring.

The hydrodynamic stiffness of the system is shown in Fig. 5.10. The hydrodynamic stiffness, given in the theory section, only exists in heave, pitch, and roll as there is no hydrodynamic stiffness provided in yaw, surge, or sway. The mooring stiffness in heave, pitch, and roll should be added to the hydrodynamic stiffness to get the total stiffness of the upper floating body. The stiffness in all six degrees of freedom are given in Tab. 5.1, for the three sources of stiffness: hydrostatic, mooring, and the suspension system. Two separate stiffnesses are provided for the mooring system: (1) at the undisplaced position of 0 surge and sway offset and (2) at an extreme surge offset of 33.4 m representing a nominal extreme surge force of 4000 kN. It is important to consider both the non-displaced system stiffness and extreme surge displacement as the mooring system surge stiffness increases with increasing surge offset. For the suspension system 4 designs are given for: the Original Design, Design A, Design B, and a design with a counter weight depth of 200 meters. The suspension system with a counter weight depth of 200 meters is given to demonstrate how the suspension system stiffness will decrease for systems with a large distance between the counter weight and floating platform.

Table 5.1: Suspension system, mooring system, and hydrostatic stiffness for the three different designs.

Operational Stiffness	C_{11} (N/m)	C_{22} (N/m)	C_{33} (N/m)	C_{44} (N m/rad)	C_{55} (N m/rad)	C_{66} (N m/rad)
Hyrdostatic (Original Design)	0	0	9.23E5	2.70E9	2.70E9	0
Hydrostatic (Design A)	0	0	9.23E5	1.51E9	1.51E9	0
Hydrostatic (Design B)	0	0	9.23E5	2.46E9	2.46E9	0
Mooring (Zero Surge)	5.32E4	5.32E4	5.61E4	2.20E8	2.20E8	1.21E8
Mooring (Extreme Surge)	3.04E5	-	2.83E4	3.07E8	-	2.44E8
Suspension System (Original Design)	1.57E8	1.81E8	3.04E8	7.81E9	9.03E9	1.05E10
Suspension System (Design A)	1.03E8	1.19E8	2.78E8	7.15E9	8.31E9	6.88E9
Suspension System (Design B)	6.11E7	7.04E7	2.32E8	5.98E9	6.87E9	4.10E9
Suspension System (200m CW Depth)	2.28E7	2.65E7	1.51E8	3.89E9	4.10E9	1.53E9

A review of the stiffnesses of the system can be used for a preliminary design analysis. This design analysis can identify the natural frequencies of the system. Since the suspended counter weight and suspension system is novel, it is important to perform a natural frequency analysis to determine what effects the suspension system stiffness has on the multi-body design.

The mooring, hydrostatic, and suspension stiffness are of different magnitudes. The mooring stiffness is relatively low and an order of magnitude lower than the hydrostatic stiffness. The largest relative stiffness of the mooring system compared to the hydrostatic stiffness, is between Design A's hydrostatic pitch stiffness and the extreme mooring pitch stiffness, which is 21% of the hydrostatic pitch stiffness. This indicates that it is important to consider the effect of the mooring stiffness for some of the DOF, but as a first approximation the mooring stiffness can be neglected.

The suspension system surge, sway and heave stiffness is relatively high compared to the hydrostaic and mooring stiffness in surge, sway, and heave. The stiffness of the systems in pitch and roll are closer. The stiffness of the suspension system in yaw is larger, however for increasing counter weight depths, the system stiffness decreases. To analyze the influence of the suspension system stiffness on the multi-body or rigid-body behavior the two-body natural frequencies are analyzed.

5.7 Natural Frequencies and Periods

The un-coupled equation of motion for the muti-body system is given in Eqn. 4.10. The coupled or un-coupled natural periods of the rigid body are given by Eqn. (7.9). It is important to consider coupling for the pitch degree of freedom, since for the original design, with coupling between pitch and heave, the pitch natural period is found to be 31.0 s, while without coupling the natural period is 38.4 s. The original design's heave natural period with coupling was 28.52 s and without coupling was 28.56 s. It can be assumed that the heave, surge, sway, and yaw natural period can be calculated as un-coupled single degree of freedom systems.

$$T_{nii} = 2\pi \left(\frac{M_{ii} + A_{ii}}{C_{ii}} \right)^{\frac{1}{2}} \tag{5.1}$$

$$f = \frac{1}{T_n} \tag{5.2}$$

Three separate representations of the floating system will be used to estimate the natural periods. The three methods are used so that the rigid-body natural periods can be compared to the multi-body natural periods. Simplifications are made to represent the system in the three following ways: as a 6 DOF rigid-body mass-spring system for the entire floating system, as a 6 DOF rigid-body mass-spring system for the counter weight suspension system connected to a rigid floating platform, and as a 1 DOF two-body mass-spring system for multi-body system.

First, the coupled rigid body natural frequencies will be given for the three systems in both mooring configurations, ignoring the stiffness of the suspension system and using one mass to represent the entire system(Tab. 5.2).

Table 5.2: The coupled rigid-body natural periods for all 6 DOF.

Natural Period (s)	T_{11}	T_{22}	T_{33}	T_{44}	T_{55}	T_{66}
Original Design Zero Platform Offset	131	131	27.7	25.3	25.3	80.3
Original Design Extreme Platform Offset	54.2	316	28.1	25.2	23.98	58.0
Design A Zero Platform Offset	117	117	24.7	33.4	33.4	75.5
Design A Extreme Platform Offset	56.7	278	25.1	28.9	33.4	53.2
Design B Zero Platform Offset	116	116	24.7	34.1	34.1	75.4
Design B Extreme Platform Offset	55.4	279	25.1	30.0	34.1	53.2

Next, the suspension system natural periods are given assuming the floater is fixed and cannot move. This demonstrates the natural periods of a counter weight suspension system that has a rigid boundary condition (Tab. 5.3). As a result of the assumption these natural periods will not represent the true natural periods of the system, but they will provide an estimate of the natural frequency associated to the suspension system. The natural periods of the system in surge, sway, and heave are low and below 2 seconds. The natural periods of the suspension system in roll, pitch, and yaw are slightly higher and in the regime of wave forcing, between 6 and 8 seconds. As a result it will be important to examine these natural periods and wave periods close to the ones discussed. An ultimate limit state analysis is performed to determine if these natural periods are observed in the time-domain numerical model.

Table 5.3: The natural frequencies of the counter weight suspension system if the floating platform were fixed and acted as a rigid boundary condition.

Natural Period (s)	T_{11}	T_{22}	T_{33}	T_{44}	T_{55}	T_{66}
Original Rigid Suspension System	1.49	1.38	1.12	7.13	6.63	5.82
Design A Rigid Suspension System	1.52	1.42	0.99	6.93	6.43	5.82
Design B Rigid Suspension System	1.96	1.83	1.08	7.56	7.05	7.48

Last, the uncoupled two-body natural periods in heave and yaw are given in Tab. 5.4. These natural periods will give insight as to if if the suspension system stiffness has an effect on the rigid-body natural periods and if the floating platform hydrostatic stiffness has an effect on the suspension system natural periods.

The flexibility of the counter weight suspension system was shown to have an effect on the natural period of the suspension system and a small effect on the natural period of the entire system. For example the natural frequency of the system in heave increased from 27.7 s to 28.2 s and the natural period of the body in yaw increased from 80.3 to 82.6. While the larger natural period increased the small natural period associated to the suspension system decreased. There are two modes of oscillation for the two bodies: in phase and out of phase. The low natural periods describe motion of the bodies that oscillate out of phase while the high natural periods describe body motion oscillating in phase.

Table 5.4: Comparison between the rigid-body and the multi-body periods.

Natural Period (s)	Suspension Rigid T_{low}	Total System Rigid T_{high}	Multi-Body T_{low} (out of phase)	Multi-Body T_{high} (in phase)
Original Design Heave	1.12	27.7	0.80	28.2
Original Design Yaw	5.82	80.3	4.36	82.6

Chapter 6

Hydrodynamic Time-Domain Numerical Model

6.1 Motivation

A time-domain approach is required as it captures the nonlinear aerodyanimc and hydrodynamic drag effects effectively. A multi-body approach in the time-domain is the most practical and provides a complete solution to the problem. Using a time-domain simulation allows for a multi-body to be modeled using lumped bodies connected through finite-elements. This multi-body model allows for the tensions in the suspension lines to be determined. It is necessary to calculate the suspension system line tension to demonstrate that the design meets the design tension requirements. To get the appropriate line tension in the suspension lines, drag forces on the counter weight need to be considered. These drag forces are applied to the counter weight body and then transferred through the suspension lines. Also, high frequency vibration in the suspension lines can be accounted for by using a multi-body approach.

6.2 Model Description

The TetraSpar floating wind turbine is modeled using a servo-aero-hydro-dynamic system in the time-domain. The multi-body analysis consisted of four rigid bodies: the floating platform, counter weight, nacelle, and hub. The hub is connected to the wind turbine blades and aero-servo-elastic code in SIMA is used to model the aerodynamic performance of the wind turbine. The bodies are connected using finite elements through the RIFLEX module. The counter weight is connected to the floating platform as it is depicted in Fig. 3.1 using finite elements in RIFLEX. The hydrodyanmics of the counter weight are modeled using Morison elements to account for drag and added-mass. The floating platform

also uses Morison elements for drag, but the added mass and potential damping are accounted for using the results from HydroD. The tower and turbine use a model of the DTU 10 MW RWT [10].

To perform a hydrodynamic analysis of the TetraSpar a first-order potential flow model was build for use in SIMO/RIFLEX [34, 35]. As discussed in the theory section, second-order forces are relatively small compared to first-order forces [35] and not considered in this study. A panel mesh was created for the floating platform to compute the potential flow solution. The creation of a mesh follows a typical procedure discussed in [14, 12]. The panel mesh, seen in Fig. 6.1, consisted of 4862 panels with an average panel size of 1 m^2. The potential flow solution is used to account for diffraction and radiation since the floating platform consists of a complex geometry. Since the counter weight is located 80 m or more below the MWL and is composed only of slender elements, the diffraction and radiation effects are negligible. The model geometry created in Genie was input into HydroD to obtain the potential flow hydrodynamic solution for the floating platform of the original design; see in Fig. 6.1. The potential flow solution was taken from the Original Design mesh and used for all of the parametric study cases. For the ultimate limit state analysis an alternative mesh was built to represent the geometry of the alternative Desigsn A and B; see Fig. 6.2. From the hydrodynamic analysis, the added mass and damping are used as inputs to SIMA which performs multibody simulations in the time domain.

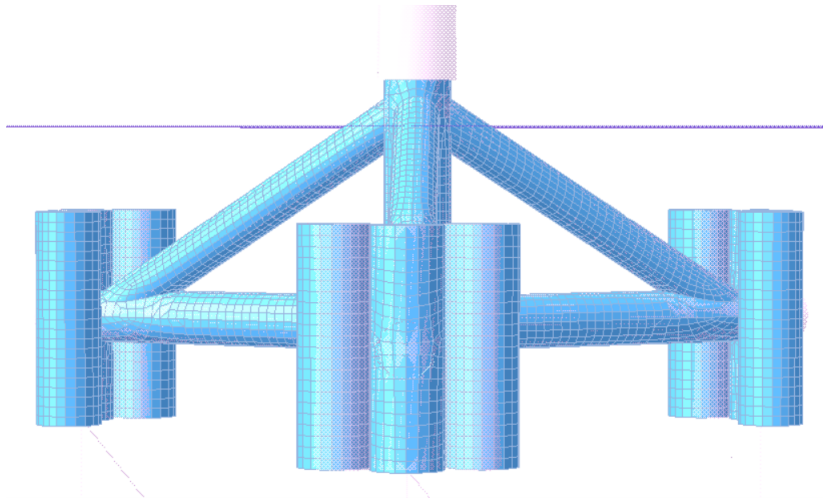

Figure 6.1: The panel mesh of the upper floating platform for the Original Design in HydroD.

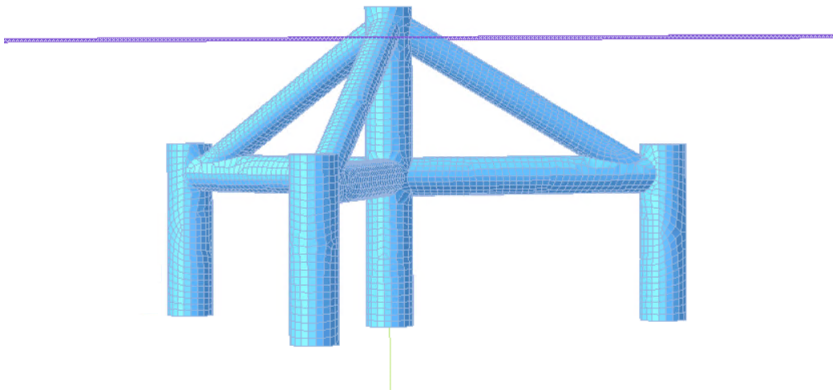

Figure 6.2: The panel mesh of the upper floating platform for the alternative Designs A and B in HydroD.

Model dimension for the counter weight mass, inertia, COG, COB, and geometry are given in the previous sections. The model verification in SIMA uses the DTU 10 MW Test Turbine. All other simulations use the DTU 10 MW Reference Wind Turbine.

6.3 Model Calibration

To verify the numerical model the 1:60 scale model tests were upscaled to full scale results using Froude scaling. Then a system was build in SIMA using the DTU Test Turbine and original TetraSpar support structure. The hydrodynamic drag coefficients were modified so that the drag properties of the model scale tests matched the numerical model. It was decided only tune damping coefficients and not stiffness or natural frequencies. Natural frequencies were not tuned because there was no physical reason that the water plane stiffness or mass of the system should be different from the values reported in the DTU DHI test campaign [23]. Differences in natural frequency are likely to arise from differences in the hydrostatic dynamic stiffness of the structure. The stiffness is highly dependant on the location of the MWL relative to the position of the upper floating platform. Small changes in vertical location of the water line will cause large changes in stiffness as the reported MWL is located at the geometrical transition where the water will transition from intersecting four members to only one. The MWL for the numerical model was set at the level shown in Fig. 3.5 to match the numerical model used by DTU [23].

6.3.1 Added Mass and Drag Coefficients

The added mass and drag coefficients, found in Tab. 6.1, were selected when calibrating the numerical model to match the DTU DHI tests. Where PF indicates that the added mass

was included from the potential flow soluiton.

Table 6.1: The coefficients of quadratic drag, linear drag, and added mass for the Morison elements used in SIMA.

Parameter	Equivalent Diameter (m)	Quadratic Drag Coefficient		Linear Drag Coefficient		Added Mass Coefficient	Potential Damping
Normal/Tangential	-	Normal	Tangential	Normal	Tangential	Normal	-
Center Column	6.6	0.9	0	0.0001	0	PF	Yes
Radial Brace	5.4	.5	0	0.0054	0	PF	Yes
Diagonal Brace	4.5	.5	0	0.0054	0	PF	Yes
Tank Set	6.6	1.1	0.1	0.0006	0	PF	Yes
Counter Weight Member	3	1.15	0.1	0.0012	0.0006	1	No

6.3.2 Calibration Discussion

The numerical model used both linear and quadradic damping coefficients to build a model that behaves similar to the physical system. To calculate these damping coefficients, first the linear and quadratic damping coefficients, b_1 and b_2, were taken from the DTU experimental free decay tests. Using these damping values coefficients were first tuned to match the heave damping coefficient using Eqn. (6.1).

$$b_1 = \sum_{Members} \frac{1}{2}\rho C_{DQ} D L \tag{6.1}$$

Once the heave damping was calibrated the remaining tuning was performed by visually inspecting the model and making changes that made physical sense. For example the normal quadratic drag coefficients were decreased for the diagonal and radial brace because of their proximity with one another. Being located close together the shielding effect is accounted for by modifying the drag coefficients. The drag coefficient of the tank set is increased to account for the effect of the cluster of three tanks. The counter weight drag was increased to account for the extra material of the counter weight joints. The linear drag coefficients were added to get a better fit with the experimental results. It should be noted that these drag coefficients are assumed to be constant, but in reality are not constant and depend on the Reynolds number which changes for changing velocities.

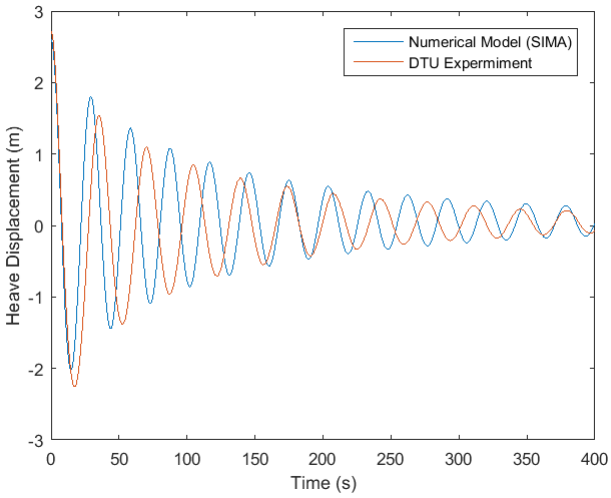

Figure 6.3: A comparison of the heave free decay tests for the upscaled model scale tests and the numerical model.

The experimental heave decay in Fig. 6.3 showed a nonlinear hydrostatic stiffness. The excursions in the negative direction were larger than the excursions in the positive direction compared to the excursions caused by a single stiffness. This is due to the fact that the hydrostatic stiffness increases for positive heave displacement and decreases for negative heave displacement. The differences in natural frequency are likely from small differences in the assumed MWL and influence from experimental equipment.

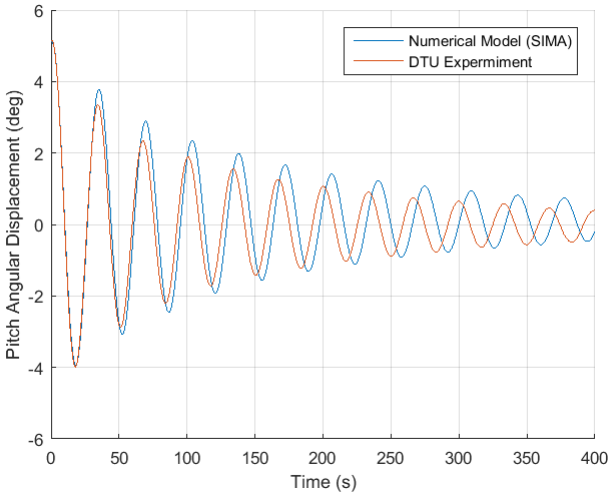

Figure 6.4: A comparison of the pitch free decay tests for the upscaled model scale tests and the numerical model.

The experimental pitch decay in Fig. 6.4 showed a larger damping value compared to a system with drag coefficients of 0.7. To match the experimental results it was required to increased counter weight damping coefficient to 1.15. One possible explanation for the increased damping value is that the electrical cables from experimental equipment resulted in additional damping.

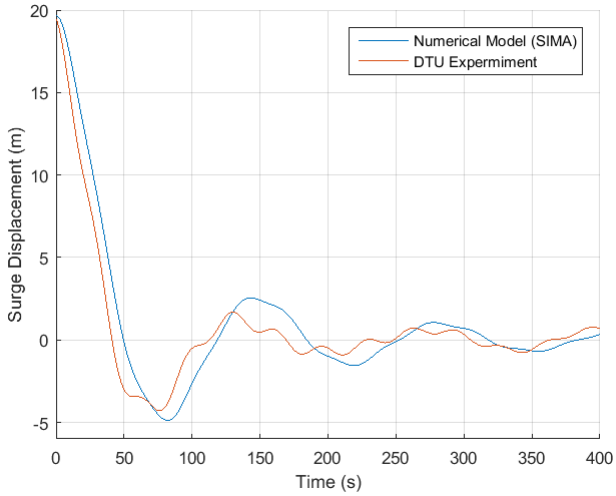

Figure 6.5: A comparison of the surge free decay tests for the upscaled model scale tests and the numerical model.

The experimental surge decay in Fig. 6.3 showed coupling between the surge and pitch DOF. This coupling is under-predicted in the numerical modeling. Again an explanation for increased coupling can be provided by additional stiffness of the electrical cables for the experimental equipment. A visual inspection shows that the quadratic damping could be increased and linear damping decreased to obtain a closer fit, however it was decided to use a combination of linear and quadratic that would result in a compromise between calibration in pitch and surge.

Table 6.2: Mooring and seafloor contact parameters.

Mooring Parameter	Value
Hydrodynamic Diameter	0.333 meters
Normal Quadratic Drag Coefficient	1.3
Axial Quadratic Drag Coefficient	0.4
Normal Linear Drag Coefficient	0.0005
Normal Added Mass Coefficient	1.6
Axial Added Mass Coefficient	1.2
Seafloor Normal Contact Stiffness	34.4 kN/mˆ2
Seafloor Normal Contact Damping	5.1 kNs/mˆ2
Seafloor In-Plane Contact Axial Stiffness	34.0 kN/mˆ2
Seafloor In-Plane Contact Axial Friction Coefficient	0.74
Seafloor In-Plane Contact Axial Damping	5.08 kNs/mˆ2

In addition to calibrating the coefficients of drag to match the surge decay, the mooring line properties were also calibrated. These mooring line properties were determined by first estimated using OrcaFlex documentation [36], then tuned qualitatively to achieve a better match of the surge decay. The seafloor contact parameters are important to get an appropriate representation of the mooring system line tension behavior.

Chapter 7

Parametric Study of the Counter Weight Suspension System

The main goal of this parametric study is to decrease counter weight mass, as it is assumed this will directly influence the system cost. A lighter counter weight will require less material to manufacture. In addition to decreasing the cost of design, decreasing the mass can decrease the cost and complexity associated to installation and transportation.

For the TetraSpar floating offshore wind turbine (FOWT) an initial parametric study is conducted to determine the optimal mass and depth of the counter weight. Typical design requirements of FOWTs include: nacelle acceleration, platform pitch angle, and rigid-body natural frequencies. In addition to these standard FOWT design requirements, the unique design requirements of TetraSpar suspended-counter-weight system are outlined. The tensions in the counter weight suspension lines will be investigated to determine the minimum tension experienced in any of the lines as well as to provide an estimate of fatigue performance.

7.0.1 Volume Constraints

To keep the same static floating platform draft about the mean water level, when decreasing counter weight mass, the buoyancy of the floating platform is decreased proportionally to the decrease in system weight. The weight decrease in the floating platform is assumed to be linear and related to a decrease in the size of buoyancy tanks. The total volume of all nine buoyancy tanks in the original design is 6650 m^3, this volume is assumed to be the limit to which the floating platform's volume can decrease. The buoyancy tanks for the full scale design have a mass per buoyancy force of 20.9 kg/kN. This ratio is used to decrease the floating platform mass for the given decrease in required buoyancy force. The change in mass and volume of the floating platform are given by the following equations, where CW denotes the counter weight, CH the suspension chain, O an original design parameter,

and F the floating platform with turbine.

$$\Delta V_F(z_{cw}, m_{cw}) = \frac{M_{CW} + M_{CH} + M_F - M_{O,CW} - M_{O,CH} - M_{O,F}}{\rho_{water}} \tag{7.1}$$

$$\Delta M_F = \Delta V_F \frac{M_{tank}}{V_{tank}} = \Delta V_F 210 kg/m^3 \tag{7.2}$$

7.1 Simplified Analytic Parametric Study

The following analytic equations can be derived to represent various system parameters dependant on the independent variables of the counter weight mass and the depth. First the analytic solution of mass, inertia, added mass, pitch stiffness, and natural periods are used to determine the effect of lowering or raising the counter weights depth or mass. In these analytic equations it is assumed that the added mass and COB of the floating structure, does not change. The natural period in any degree-of-freedom for a floating structure can be calculated from equation 7.9. An increase in mass or inertia, M, or the added-mass and added-inertia, A, cause an increase in period. For the stiffness, C, an increase in stiffness causes a decrease in period. The COG and COB of the structure can be calculated from the following equations:

$$COG(z_{cw}, m_{cw}) = \frac{z_{cw} m_{cw} + COG_{CH} M_{CH} + COG_F M_F}{M_F + M_{CH} + m_{cw}} \tag{7.3}$$

$$COB(z_{cw}, m_{cw}) = \frac{z_{cw} V_{cw} + COB_{CH} V_{CH} + COB_F V_F}{V_T} \tag{7.4}$$

The inertia of the system is dependant on the original inertia. When the mass is changed the inertia of the counter weight, about its COG_{CW}, scales linearly. When the counter weight depth is changed the inertia of the system increases due to the increased moment arm of the gravitational force of the counter weight.

$$I_{55}(z_{cw}, m_{cw}) = I_{Ocw,55} \frac{m_{cw}}{M_{OCW}} + m_{cw} z_{cw}^2 + I_F \tag{7.5}$$

An analytic expression for the added mass of the counter weight can be derived by considering the added mass of three cylindrical beams. Here the analytic solution matched the numerical added mass closely and the numerical added mass value was used. Since the counter weight structure does not change, the added mass change is dependant on the moment arm from the center of rotation to the equivalent location of the beams. This moment arm is calculated using the radius of gyration from the z axis and the depth of the counter

weight by taking the: $\sqrt{z_{cw}^2 + R_{g,CW}^2}$.

$$A_{55}(z_{CW}, m_{CW}) = A_{O,F,55} + \frac{A_{OCW,55}\sqrt{z_{CW}^2 + R_{g,cw}^2}}{\sqrt{z_{O,cw}^2 + R_{g,cw}^2}} \tag{7.6}$$

An analytic expression for the system pitch stiffness follows from the pitch equation discussed in (4.1). Since the position of the floating platform, relative to the MWL, remains constant, the water plane area integration term also remains constant. As a result, the only changes in pitch stiffness come from the change in system COG, COB, mass, and volume.

The pitch stiffness is an important design parameter. It is desired to keep the pitch at rated power below 5°. The analytic equation for pitch stiffness is used to keep pitch stiffness at the desired value while varying the independent variables z_{cw} and m_{cw}. In this way the pitch design requirements can be met while decreasing mass and counter weight position.

$$C_{55} = \rho g V_T(COB(z_{cw}, m_{cw}) - COG(z_{cw}, m_{cw})) + \rho g \int\int y^2 ds \tag{7.7}$$

The analytic solution for the system period in heave and pitch is checked to ensure that the period of the system is outside of the environmental forcing periods. The pitch and heave DOF are coupled together. It is important to considering the coupling between heave and pitch while calculating the natural periods as it is found to have a significant effect on the resulting pitch natural period. It is sufficient to consider only heave and pitch in the coupling matrix since the natural period of surge is very low and coupling between pitch and the other degrees-of-freedom is small.

$$T_{nii} = 2\pi \left(\frac{M_{ii} + A_{ii}}{C_{ii}} \right)^{\frac{1}{2}} \tag{7.8}$$

$$T_{n33,55} = 2\pi \left(\frac{M_{33,55} + A_{33,55}}{C_{33,55}} \right)^{\frac{1}{2}} \tag{7.9}$$

7.2 In Depth Parametric Study Using The Time Domain

The environmental conditions considered for the parametric study are average rated conditions experienced during operation. The rated conditions described in Tab. 9.4 are used for the parametric study. It was decided to use rated-environmental conditions for the parametric study since these conditions result in the largest operational design thrust. Average conditions were used to approximate fatigue in the suspension lines. Using average-rated-

Table 7.1: The properties that are changed or held constant during the parametric study.

Parametric Study Variable	Changing or Fixed
Mean Pitch Offset at Rated Power	Fixed
Hydrostatic Pitch Stiffness	Fixed
Floating Platform Draft	Fixed
Counter Weight Depth	Increasing
Counter Weigh Mass	Decreasing
Counter Weight Volume	Fixed
Floating Platform Volume	Decreasing
Floating Platform Mass	Decreasing

environmental conditions would give results that are similar regardless of the selected design environment, since pitch motion is dominated by wind loading which is a function of the turbine used. In this way results general results are applied that are valid for less extreme environments. It is still important to consider the extreme environmental conditions and this is done in the following ultimate limit state design check.

The properties of the design that are adjusted and held constant are listed in Tab. 7.1. This study varies counter weight mass and accordingly changes counter weight depth, floating platform volume, and floating platform mass to maintain: (1) constant hydrostatic pitch stiffness and (2) constant draft of the floating platform about the mean water level. To maintain constant hydrostatic pitch stiffness while decreasing counter weight mass the counter weight depth is increased.

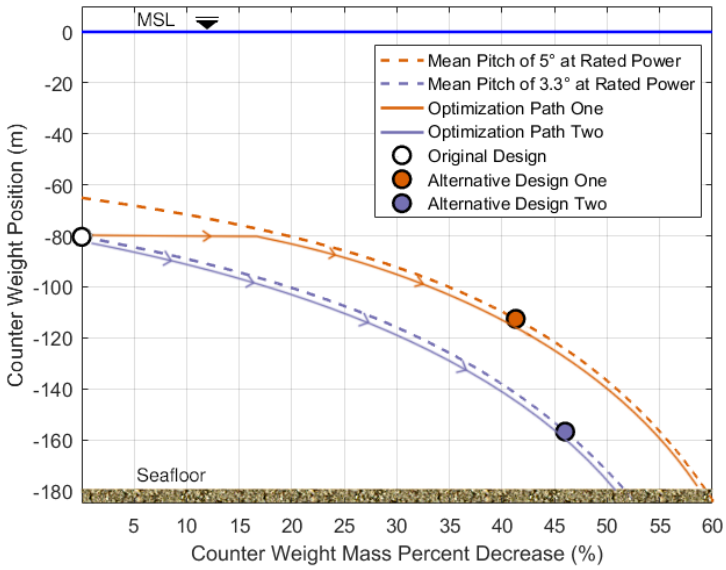

Figure 7.1: Design paths starting from the original design and decreasing counter weight mass.

7.3 Parametric Paths

The parametric study of the counter weight mass investigates two values of pitch stiffness: 1.6E9 and 2.6E9 $N \cdot m/deg$. These stiffnesses represent two different degrees of stability: (I) a decreased stiffness that results in a mean pitch offset of 5° at rated power and (II) the original design stiffness that results in a pitch offset of 3.3° at rated power. The parametric study for these two stiffnesses can be seen in Fig. 7.1.

Design Path (I) maintains a constant pitch stiffness of 1.6E+9 $N \cdot m/deg$. This path has a larger initial mass decrease, but a decreased stability compared to the original design. It can be observed that initially, to maintain constant hydrostatic stiffness, the counter weight only needs to be lowered slightly while decreasing mass.

A second design Path (II), is analyzed with the same hydrostatic pitch stiffness of the original design (2.6 $N \cdot m/deg$). Path (II) requires a deeper counter weight to achieve the same decrease in mass compared to Path (I). These two stiffness were investigated to analyze the dynamic behavior of two systems with different pitch stiffness. Path (II) maintains the decreased mean pitch offset of the turbine, while obtaining similar values for decreased mass. The results along these paths are next compared to determine the limitation of decreasing counter weight mass or position.

To compare the different systems along the design path, single 4,000 second simulations

were run using the same wave and wind time series for each design. This gives a direct comparison while allowing for a quick parametric analysis. More simulations were not required as the trend in the results show a smooth correlation between parameters. Extreme statistics represent the expected behavior of extreme responses in comparison to the alternative designs. In this way the expected behavior of alternative designs can be estimated relative to the original design.

7.4 Results

7.4.1 Suspension System Line Tension

The main design limitation encountered, when decreasing mass, was that the minimum line tension, in the counter weight suspension line, decreased below zero. Decreasing the counter weight mass decreases the static tension in the lines, bringing the design closer to the limit. For the two design paths, final alternative designs were selected having a k value that satisfies Eqn. (3.2). The original design had k values of 17.2 for average rated conditions. This shows that there is potential room for reduction of this value. Design alternative (I) and (II) had k values, for the single hour simulations, of 5.6 and 5 respectively.

Figures 7.2 and 7.3 show the line tension of Line 1, the line that experiences the smallest tension, for design Path (I) and (II) respectively. For design Path (I) the counter weight tension at 80 m depth starts lower than design Path (II) because Path (I) begins with a smaller initial mass. In design Path (I) the minimum line tension decreases below zero at a counter weight depth of 153 meters. For design Path (II), the line tensions do not decrease below zero, however they do decrease to 1200 kN at a depth of 170 m. Along Path (II), the counter weight is capable of being placed at a greater depth, due to its larger initial mass, compared to design Path (I) resulting in a similar mass decrease.

The parametric study was run for a pitch direction of 90° degrees, which accounts for the most extreme loads on the mooring system. As identified the critical pitch angle is smaller for a pitch direction of 60°. The minimum line tensions experienced are expected to be on average 9% smaller for wind pitch direction of 60°.

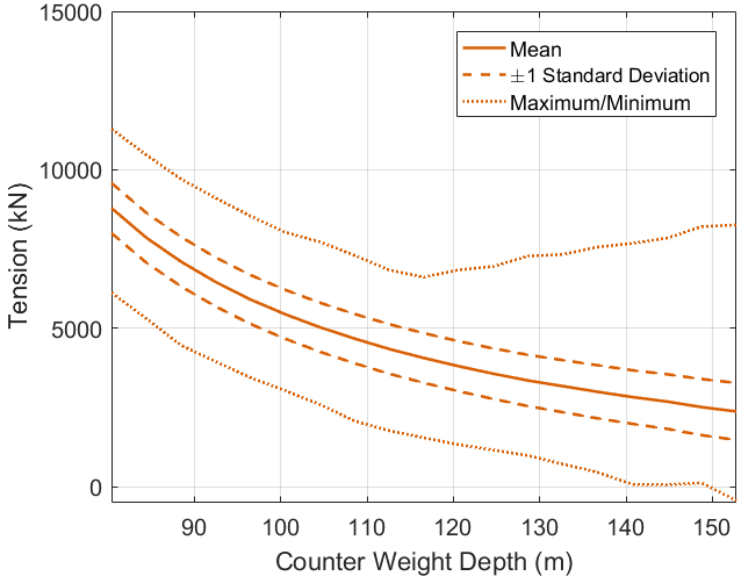

Figure 7.2: The line tension in Line 1 for Design Path (I), increasing counter weight depth and decreasing counter weight mass along the line of constant stiffness 1.6E9 $N \cdot m/deg$.

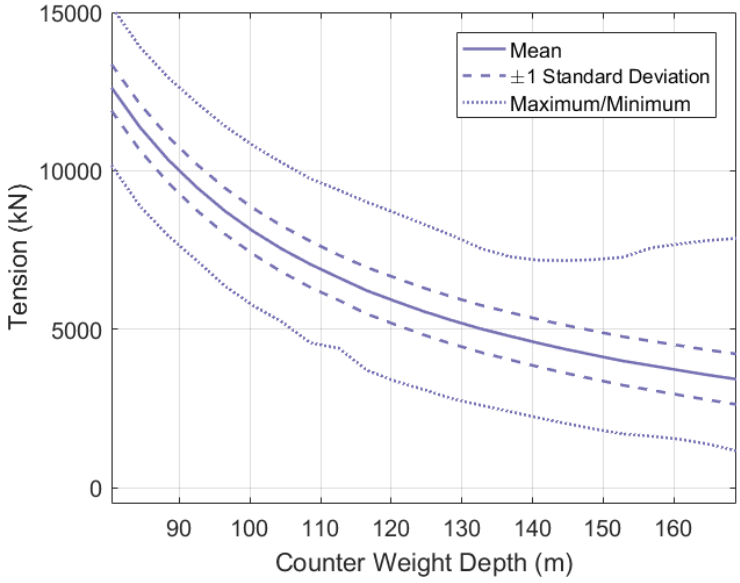

Figure 7.3: The line tension in Line 1 for Design Path (II), increasing counter weight depth and decreasing counter weight mass along the line of original design stiffness 2.6E9 $N \cdot m/deg$.

7.4.2 Fatigue Damage From Rated Conditions

The suspension chains must be able to transfer the static-vertical-gravitational forces of the counter weight in addition to dynamic-vertical forces caused by wave induced heave motion. The suspension chains must also transfer the dynamic-horizontal pitch restoring force during pitch offset. The counter weight's draft will effect the chain tensions due to the resulting change in geometric angle between the chains and the vertical axis. When the counter weight draft is increased the suspension line's ability to transfer vertical forces improves due to the change in angle that the suspension line makes the vertical axis. The opposite occurs when the counter weight's draft decreases the suspension line's ability to transfer horizontal forces improves. Changing the draft of the counter weight will effect the fatigue experienced by the suspension lines as it experiences changes in dynamic horizontal and vertical forces.

Fatigue damage was calculated in the counter weight suspension lines and normalized with respect to the original design's fatigue value. The fatigue was calculated using Miner's rule on the one-hour rated-wind simulations described in Tab. 3.5. The sea sates used were the normal sea states described by the average wave height and period of rated wind speeds. These conditions were used to estimate the fatigue performance for each design along the design path of decreasing counter weight mass and position.

One consequence of decreasing the depth of the counter weight is an increase in fatigue damage in the counter weight suspension lines (Fig. 7.4). This consequence can be seen by the larger fatigue value along Path (II), which has a larger counter weight depth for a given system mass compared to Path (I). The fatigue damage begins to rise exponentially as the mass decreases to a point where the tension in the counter weight suspension lines cannot be maintained above zero, representing an unstable system limit. A mass decreases of 41% and 46% lead to increases in fatigue damage of 3% and 25% for Path (I) and (II), respectively. Fatigue is not expected to be a limitation in increasing the depth of the counter weight. The sharp rise in fatigue damage at larger counter weight depths is associated to larger extreme deviations from the mean tension.

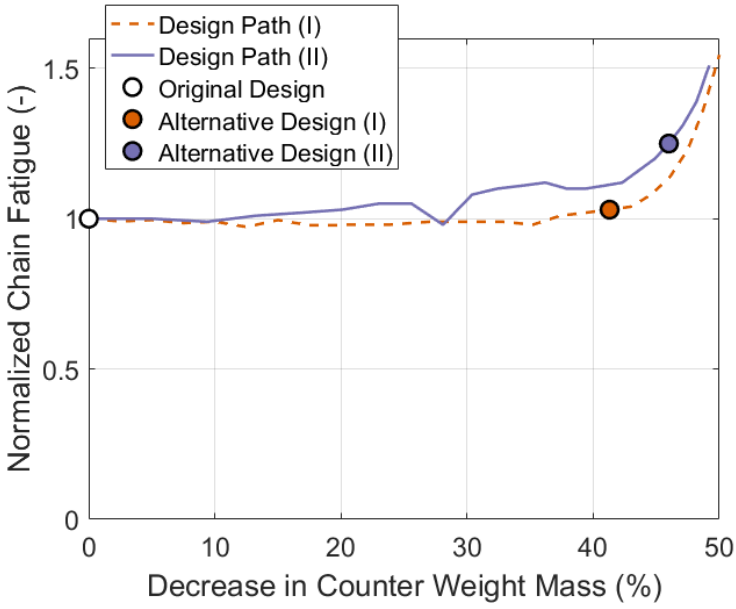

Figure 7.4: Normalized counter weight suspension system line fatigue for both design paths.

7.4.3 Nacelle Acceleration

Nacelle acceleration can be directly related to the loads and fatigue experienced by the wind turbine. The wind turbine on the Hywind spar represents 60% of the cost for the total floating structure [37]. Due to large relative cost of the turbine, it is important to minimize the acceleration experienced by these components to protect this investment. The nacelle acceleration is plotted against percent counter weight mass decrease (Fig. 7.5); this is done to show the effects on nacelle acceleration when decreasing system mass. The increase in nacelle acceleration standard deviation for alternative designs (I) and (II) was 12% and 13% for a mass percent decrease of 41% and 46% respectively.

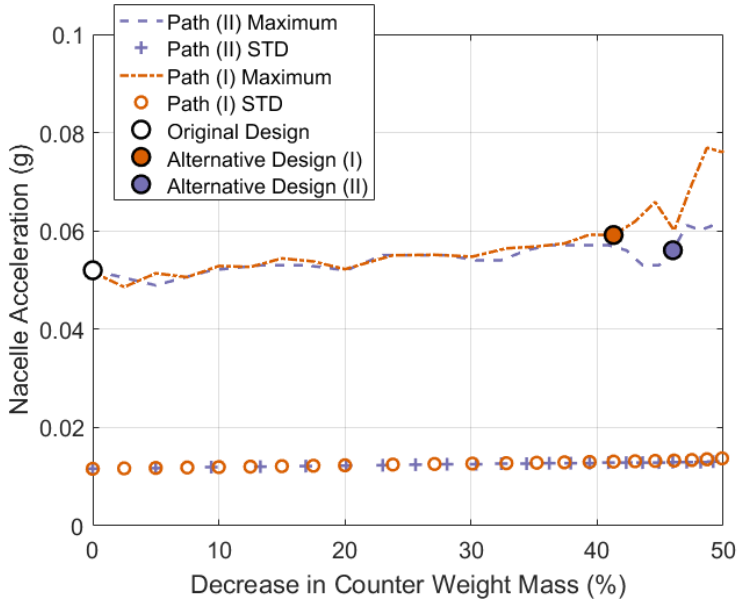

Figure 7.5: Nacelle acceleration for both design paths.

It is clear that nacelle acceleration increases for decreasing system mass. This is expected since the system has less mass to resist the acceleration, while the environmental loads do not change. The system moment of inertia in the direction of pitch increases for both design paths after a counter weight mass decrease of 20%. This suggests that for normal operational conditions the nacelle acceleration is governed by mass and not hydrostatic inertia. Hydrostatic pitch stiffness is seen to have little effect on system acceleration during rated conditions since the differences in nacelle acceleration standard deviation only differed by 2% for percent mass decreases below 40%. This small difference is expected to be attributed to the larger system inertia of design Path (II). This suggests that the hydrostatic pitch stiffness does not have an effect on limiting nacelle acceleration.

Chapter 8

Alternative Designs from the Parametric Study

8.1 Design Description

The three designs: the original and the two alternative designs (I) and (II), found from the design paths, are compared. These designs represent designs within the design limits, during rated conditions. As rated conditions are used for the parametric study, the alternative designs are appropriate for mild environmental conditions and not extreme environmental locations. The in-ability to meet the design requirements for extreme conditions will be demonstrated in the ultimate limit state check. To calculate the new natural frequencies in pitch and heave, a potential flow model was built using the same procedure as the original design. This is required determining the hydrodynamic properties of the alternative designs. The results from the parametric study are recorded in Tab. 8.1. A comparison between the TetraSpar and a more conventional spar, designed by Wenfei [22] for the DTU 10 MW RWT, shows that with similar stiffness and drafts the TetraSpar support structure is able to weigh 35% less; see Tab. 8.2.

Two design alternatives have been proposed, one with the same hydrostatic stiffness of the original design and one with decreased hydrostatic stiffness. The alternative design (I) has decreased hydrostatic stiffness and is able to decrease system mass by 30% with a 3% increase in fatigue of suspension line, a 12% increase in nacelle acceleration, and a 56% increase in mean pitch offset during production at rated wind conditions. The alternative design (II) has the original hydrostatic stiffness and is able to decrease system mass by 32% with a 25% increase in the fatigue of suspension Line 3, a 13% increase in nacelle acceleration, and a 3% increase in mean pitch offset during production at rated wind conditions.

Table 8.1: Proposed system properties of the TetraSpar with the DTU 10 MW RWT.

Design Properties Observed at Rated Power	Original Design	Design (I)	Design (II)
Mean Pitch Offset (°)	3.23	5.05	3.32
Maximum Pitch (°)	5.93	9.01	5.86
Maximum Nacelle Acceleration (g)	0.052	0.059	0.056
Normalized Power Production (%)	100	98.8	99.7
Normalized Line Fatigue (%)	100	103	125
Min. Line Tension (kN)	10200	1770	1630
Max. Line Tension (kN)	19200	11100	9790
Line 3 Tension STD (kN)	731	781	773
Line Zero Tension Safety Factor, k	17.3	5.6	5
Heave Natural Period (s)	29.5	25.2	24.9
Pitch Natural Period (s)	28.8	40.1	41.0
Total Mass Including Turbine and Ballast (tonnes)	13000	9120	8850
Counter Weight Mass (tonnes)	8100	4740	4360
Pitch Inertia (kg m^2)	7.3E10	7.9E10	13.9E10
Pitch Stiffness (N m/°)	2.6E9	1.6E9	2.6E9
Heave Stiffness (kN/m)	920	920	920
Draft (m)	82	114	158

Table 8.2: Comparison between a conventional spar and the TetraSpar Designed for the DTU 10 MW RWT.

Design Properties	TetraSpar Design (I)	Spar
Draft (m)	114	120
Support Structure Mass (tonnes)	7900	12100
System Inertia (kgm^2)	7.9E10	12.7E10
Heave Natural Period (s)	25.2	31.9
Pitch Natural Period (s)	40.1	39.9
Pitch Stiffness (N m/°)	1.60E9	1.69E9
COGz (m)	-54.1	-74.6
COBz (m)	-34.6	-62.1

Chapter 9

Ultimate Limit State Check of Alternative Designs

In the parametric study rated wind speed conditions were tested to identify the potential for alternative designs. In the ultimate limit state analysis many separate extreme and operational cases are run to determine if the system meets the design requirements for all of the specified design cases. In addition typical design cases, a separate natural frequency investigation is performed to determine the consequences of having a suspension system natural frequency inside the expected peak wave frequencies. The original design was shown to be conservative in the operational phase. Two design alternatives were proposed, that aimed to meet design requirements, while reducing structure weight. The main design parameter, that acts as a limiting factor in reducing weight, was the cable tension. An ultimate limit state design check is performed using time-domain simulations in SIMA to test the design in a range of conditions. The ultimate limit state test is also used to determine how the alternative Designs A and B compare to the Original Design.

9.1 Cases Tested

Several design cases are specified in the IEC Standard: IEC 61400-3 - Design Requirements for Offshore Wind Turbines [25]. A reduced selection of cases are chosen to perform an ultimate limit state design. The following design cases are presented in Tab. 9.4. The selected design cases cover a range of design situations occurring during power production, emergency shut down, and parked-extreme conditions.

Table 9.1: IEC 61400-3 design cases used to investigate the ultimate limit state response of the TetraSpar. Where the following abbreviations represent the environmental design conditions: Normal Turbulence Model (NTM), Extreme Turbulence Model (ETM), Extreme Wind Model (EWM), Normal Sea State (NSS), Extreme Sea State (ESS), Co-directional (COD), Unidirectional (UNI), Normal Current Model (NCM), Extreme Current Model (ECM), and Mean Water Level (MWL).

Design Situation	Case #	Wind	Waves	Wind and Wave Directionality	Current	Water Level	Other Conditions
Power Production	1.1	NTM	NSS	COD, UNI	NCM	MWL	
	1.3	ETM	NSS	COD, UNI	NCM	MWL	
	1.6a	NTM	SSS	COD, UNI	NCM	MWL	
Emergency Shut Down	5.1	NTM	NSS	COD, UNI	NCM	MWL	
Parked	6.1a	EWM Turbulent	ESS	MIS, MUL	ECM	MWL	
	6.3a	EWM Turbulent	ESS	MIS, MUL	ECM	MWL	Extreme Yaw Misalignment

In addition to the design cases from the IEC standard a separate natural frequency analysis was also run. From the initial counter weight design check, the natural periods of the rigid-body system and multi-body system were estimated. The estimates of the natural frequency identified that there were suspension system natural frequencies that overlapped with possible peak wave periods. To identify the behavior of the system when excited with the given natural frequency several wave spectrum were applied with varying frequencies to determine the extent of the excitation occurring at the estimated frequencies. Time domain simulation were run with sea states represented by peak periods between 2 and 21 seconds. The sea states considered are given in in Tab. 9.2 and are representative of the environmental conditions of Norway 5.

Table 9.2: Peak spectral period and significant wave height of sea sates considered in the natural frequency check.

JONSWAP Normal Sea State Parameters													
Tp	2	3	4	5	6	7	8	9	10	12.5	15	18	21
Hs	0.5	1	2	3	3.8	4.8	5.3	6.2	7	9.8	9	7	3

9.2 Response Variables Analyzed

As was done in the parametric study, the following floating system response variables will be analyzed in the ultimate limit state check: nacelle acceleration, suspension line tension, mooring line tension, maximum pitch angle, and maximum horizontal displacement. These response variables are checked to determine if the design limits, listed in Tab. 3.6, are exceeded.

9.3 Results

9.3.1 Natural Frequency Investigation

Simulations were run for all of the sea states in Tab. 9.2. The results of this investigation show that the critical response of the line tension is caused by extreme waves and is not driven by the natural frequency of the response of the multi-body system. Figure 9.1 shows that the most extreme response of the line tension in Line 4 is caused by extreme wave heights and not by resonance of the identified multi-body frequencies. From Tab. 5.3 it was identified that there are several natural frequencies that can be introduced due to the stiffness of the suspension system. Estimates of the natural frequencies of the suspension system were made by assuming the floating platform fixed and that only the counter weight was able to move relative to the floating body. This method showed natural periods of the original suspension system of 1.5, 1.4, 1.1, 7.1, 6.6, and 5.8 seconds respectively for the surge, sway, heave, pitch, roll, and yaw degree of freedom.

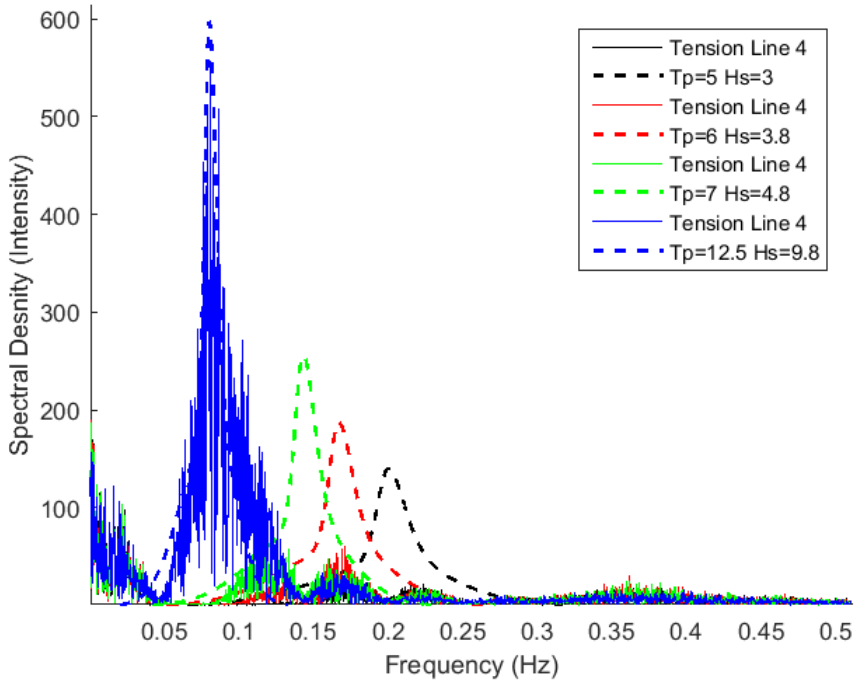

Figure 9.1: The spectral response of Line 4 tension and JONSWAP wave spectrum for each time domain simulation.

The numerical simulations were run and results are shown for select wave periods, of 5,

6, 7, and 12.5 seconds, in Fig. 9.1. Natural period peaks were identified near the analytic natural frequencies. The numerical model showed natural periods at 2.8, 4.5, 5.9, and 7.9 seconds. Although natural frequency peaks were observed associated to the suspension system natural frequencies, it was determined that the first-order wave loads had a greater influence on the most extreme response. The most extreme response occurred during the simulation with the largest significant wave height. In the simulation with the largest significant wave height, the majority of the energy in the response is associated with the first-order wave loads caused by the extreme waves. One reason for this is that extreme wave spectrum has a narrower distribution. The frequency response of this extreme wave was dominated by the applied wave frequency and not the natural frequency of the suspension system.

9.3.2 Wind Wave Directionality

For design case 6.1a and 6.3a misaligned and multi-directional waves are required to be analyzed. There are many possible wave, wind, and current combinations. It was assumed that current was always aligned with the wind direction. In the previous sections it was shown that the critical suspension line angle was minimum for pitch about 30, 90, 150, 210, 280, and 330 degrees. Damping is greater in pitch than in roll, in the local coordinate system. As a result of this non-constant damping, it is important to consider the dynamic behavior of the wind and wave misalignment in order to determine the most extreme response.

For case 6.1 several different wind-wave combinations were run to determine which one results in the most extreme response. It was found that the wind-wave direction combination that resulted in the maximum standard deviation of Line 4 tension, also resulted in the maximum nacelle acceleration and lowest line tension.

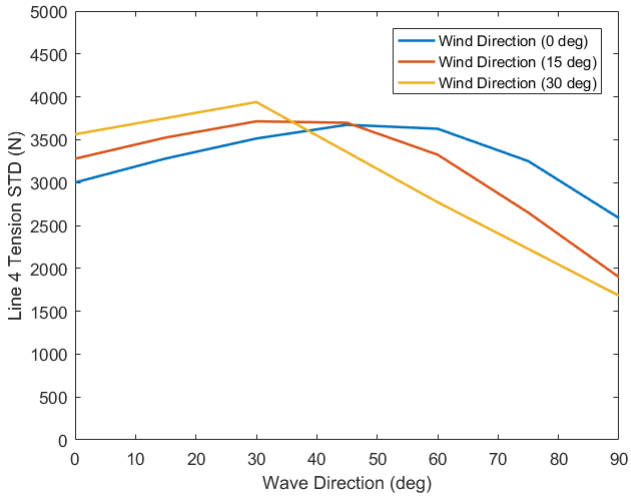

Figure 9.2: Line 4 suspension line tension standard deviation for different wind-wave directions. With the wave in degrees of misalignment clockwise from the wind direction.

Figure 9.2 shows the tension standard deviation in Line 4 for different degrees of wave misalignment. The tension standard deviation is plotted against wave direction for three different wind directions in degrees. The combination that results in the greatest line tension is when the wind is aligned and directed at 30 degrees and the waves are misaligned 30 degrees clockwise from the wind. It is expected that a combination of wind and waves that results in a rotation about one of the critical pitch directions would result in the most extreme reaction. The results shows that this is true, but that additionally some wind/wave misalignment, in addition to the wind being directed at the critical pitch angle, results in the most extreme reaction force. Once the most critical wind-wave direction combination was found for case 1.6a of the original design, it was also assumed to be the design case for the alternative designs.

9.3.3 Original Design Results for All Design Cases

The cases that result in the original design's most extreme responses are now analyzed. The cases that result in the most extreme responses are selected to be analyzed for all the alternative designs. The cases with extreme wind and waves combined the extreme 50 year wave conditions with the extreme 50 wind conditions to result in a conservative prediction of extreme conditions.

Table 9.3: Results of the ultimate limit state cases for the original design.

Design Situation	Case	Line with Minimum Tension (kN)			Maximum Platform Pitch (deg)	Nacelle Acceleration (g)
		Minimum Line Tension	Mean Line Tension	STD Line Tension		
Power Production Normal Turbulence	1.1 Vs_{Rated}	10,200	12,500	638	5.3	0.04
	1.1 Vs_{out}	9,400	13,500	1,020	2.9	0.08
Power Production Extreme Turbulence	1.3 Vs_{Rated}	9,840	12,600	743	5.8	0.05
	1.3 Vs_{out}	9,650	13,500	1040	2.9	0.07
Power Production Severe Sea State	1.6a Vs_{Rated}	6,670	12,600	1,370	5.5	0.11
	1.6a Vs_{out}	6,570	13,500	1,990	3.4	0.14
Emergency Shut Down	5.1	11,300	14,400	1,010	4.9	0.06
Extreme Environment	6.1a	-3,460	9,480	4,110	8.5	0.97
Extreme Environment Yaw Miss-Alignment	6.3a	-2,350	10,020	3,260	8.7	0.69

Extreme environmental conditions, of case 6.1a and 6.3a, result in the most critical design responses. It is seen that line tensions become negative with -3,460 kN tension in case 6.1a. These minimum line tensions are small for two reasons: there is a small mean line tension and a large line tension standard deviation. The mean line tension is low, 9,480 kN, due to a mean pitch offset from extreme-mean wind moments. The line tension standard deviation is large because of the large extreme wind and wave moment standard deviations. The maximum platform pitch angles are within the limit for all DOF suggesting that the stiffness of the system is sufficient. The nacelle acceleration is large, 0.97 g, and exceeds the design limit in the extreme environmental cases. This large acceleration is likely caused by the zero or negative line tensions resulting in snap loading.

Cases 1.1-5.1 all pass the given design requirements. It is only the extreme environmental conditions of the site Norway 5 that cause the design to exceed its design limits. The conditions at Norway five represent some of the most severe conditions experienced in the North Sea with significant wave heights of 15.6 m and extreme wind speeds of 42.9 m/s. The results are descriptive of this extreme environment and for less extreme environmental conditions other design cases may dominate.

9.3.4 Extreme Design Response for All Designs

The extreme results were found to exceed the design limits and be the most extreme for the design conditions of case 6.1a. From Tab. 9.3 it was shown that design case 6.1a resulted in the worst conditions. To perform a design check of the alternative designs the worst case condition, 6.1a, was run for the alternative designs.

The alternative designs were shown to not to pass the design requirements. The alternative designs experienced smaller line tensions because the designs make the suspension system tension less conservative. Although the alternative designs make the suspension system less conservative, the designs also were expected to reduce wave loading acting

on the structure due to removing two of the tanks. The wave loading reduction was not accounted for in the parametric study since the hydrodynamic model used the original design frequency-domain results to determine wave loading. It can be seen that the alternative designs reduce wave loading from the decrease in line tension standard deviation for Designs A & B. The decrease in wave loading was not sufficient to overcome the decrease in suspension system mean tension.

Table 9.4: Response variables for all designs during the extreme conditions of design case 6.1a.

Design	Line with Minimum Tension			Maximum Platform Pitch	Nacelle Acceleration (g)
	Minimum Line Tension	Mean Line Tension	STD Line Tension		
Original Design	-3,460	9,500	4,100	11.7	0.97
Design A	-15,900	1,900	3,600	26.2	0.82
Design B	-8,210	2,300	3,300	18.5	0.75

From Tab. 9.4 the results show that none of the designs pass the design requirements. The initial design decisions were made with the belief that the rated conditions would result in the greatest pitch motion. It was thought that the greatest mean pitch would be due to the large trust and moment experienced at rated thrust. It was show that the extreme conditions at the Norway 5 site result in more extreme platform pitch motion response.

As the original design failed to meet the design requirements, so do the alternative designs A & B. In addition to the floating platform failing to meet the design requirements the mooring system also fails to meet design requirements. The mooring system for the original and alternative designs experienced zero tension and negative tensions during extreme conditions. These zero tensions indicate that the mooring may need to be redesigned in addition to the floating platform. Different alternative designs should be investigated that increase the mass of the counter weight and raise the counter weight. It is clear that for designs with extreme environments, parametric design should use these extreme conditions as they result in the most extreme system responses.

Chapter 10

Conclusion

10.1 Conclusion

A technical description of the counter weight technology utilized by the TetraSpar floating support structure has been proposed and is investigated using analytic equations, a parametric study, and an ultimate limit state analysis. The counter weight suspension system offers the favorable operational stability of the classical spar technology, while enabling an greater distance between the COG and COB. By being designed of geometry that is favorable for mass production, this system can industrialize the offshore floating wind energy industry. The physical mechanisms behind the design and operation of the counter weight suspension system have been identified and can be used to design a system that meets the design requirements.

The several technical investigations of the counter weight suspension system have resulted in the following conclusions:

- For angles of heel less than the critical angle, the counter weight suspension system acts as a stiff-multibody system. Below the critical angle, any relative motion between the counter weight and floating platform is caused by the axial elongation of the suspension lines. The smallest critical angle, for any heel direction, was found to be 21.1° for the original design.
- When the equivalent stiffness of the suspension system is large, the hydrodynamic loading on the system can be approximated using a rigid-body assumption.
- To perform a complete design analysis, it is necessary to perform a multi-body analysis to correctly determine suspension system line tensions.
- The analytic analysis shows that the suspension system introduces additional natural frequencies into the system. These natural frequencies can be in the range of wave periods.

- The numerical model showed some excitation of the natural periods at 2.8, 4.5, 5.9, and 7.9 seconds for the original design. The additional natural frequencies were not shown to cause the exceedance of any design limits. It is shown that the line tensions that drive the design are more influenced by forcing at the extreme wave periods, opposed to resonance at the suspension system natural frequencies.

- A parametric study was conducted using a multi-body global response analysis. The limiting requirement determined in this study was that: zero line tension in the suspension system must not occur to avoid snap loads.

- A hydrostatic analysis was conducted using frequency-domain hydrostatic software. The limiting requirement determined from this analysis was that: the upper-floating platform must have sufficient stability to meet installation and transportation requirements. The requirement of having sufficient stability limited the ability to decrease the floating platform mass and volume.

- Alternative Designs (I) and (II) are determined from the parametric study and show the potential of decreasing the system weight compared to the original design and conventional spar technology. These alternative designs require temporary stability to be provided during transportation and installation in order to achieve the greatest mass decrease and take full advantage of the counter weight suspension technology. Also these designs require sites with less extreme environmental conditions compared to the ones investigated in this study.

- Alternative Designs A and B are determined from the parametric study and show the possibility of decreasing the weight of the original system. These alternative designs increase the transportation and installation stability compared to Designs (I) and (II), however they also require temporary stability to be provided during transportation and installation.

- From an ultimate limit state analysis it is found that all designs fail the design requirements related to positive line tension, nacelle acceleration, and maximum platform pitch angle. To design a system for the extreme conditions of the Norway 5 site, the demonstrated parametric study procedure can be utilized, however design case 6.1a should be used as the critical design case. To meet the extreme design conditions of Norway 5 the suspension system should be made more conservative by increasing the mass of the counter weight and decreasing the depth of the counter weight.

For sites with less extreme environments, the potential to decrease mass is large. The expected consequences from decreasing mass are expected to be small increases in nacelle acceleration and chain fatigue. Other design limits encountered are designing a upper floating platform that has sufficient hydrodynamic stability during the transportation and installation phase. To capture the full benefit of the counter weight technology alternative methods for transportation and installation are required. The original design has significant hydrodynamic stability during towing. Alternative designs (I) and (II) identified in the parametric study represent designs that require temporary stability during installation and transportation. Due to the difficulty in designing an upper floating platform that is

sable with the volume requirements of design (I) and (II) alternative designs A and B are presented. These designs require additional stability during towing and installation to meet DNVGL standard requirements, but are stable in mild environmental conditions.

The mechanisms behind successful operation of counter weight technology have been demonstrated. While the design limits were not met for the extreme conditions of Norway 5, it is possible to re-design the system to meet these requirements. A straight forward procedure is presented in the parametric study to re-design the system. The re-design of this system is expected to result in a design that has an increased mass compared to the original design. While the extreme conditions of Norway 5 require an increased design mass, the TetraSpar design can achieve large reductions in mass for less extreme environments. The mass of the original TetraSpar design is comparable to the mass of a traditional spar, however the TetraSpar technology has clear advantages in its ability to be mass produced and installed in shallow water ports.

10.2 Future Work

This work identifies design constraints encountered when utilizing a counter weight suspension system. The ultimate limit state analysis demonstrates that a redesign of the mooring system and counter weight suspension system is needed to meet the extreme environmental conditions of Norway 5. A complete stochastic analysis is required to fully understand the statistical behavior of line tension for different environmental conditions and fault scenarios. To do this an extended list of design cases should be run representing coherent gusts and additional fault cases [38, 39]. With the critical design case determined, several hour long simulations are required to determine the statistical behavior of this critial case.

Temporary stability during installation and transportation can allow for the design of a lighter support structure in mild environments. If sites are considered with more moderate environmental conditions, technology that can provide temporary stability is of interest. This technical investigation of novel installation methods can reduce system mass by taking full advantage of the counter weight suspension system technology.

Bibliography

[1] J. Jonkman P. Sclavounos S. Butterfield, W. Musial and W. Libby. Engineering challenges for floating offshore wind turbines. In *Offshore Wind Conference*, Copenhagen, 2005.

[2] A. Peiffer D. Roddier, C. Cermelli and A. Aubault. Summary and conclusions of the full life-cycle of the windfloat fowt prototype project. In *ASME 2017 36th International Conference on Ocean, Offshore and Artic Engineering*, Trondheim, 2017.

[3] Statoil to build the worlds first floating wind farm: Hywind scotland. https://www.statoil.com/en/news/hywindscotland.html. Accessed: 2017-12-15.

[4] Joachim Seel E. Baker M. Hand E. Lantz R. Wiser, K. Jenni and A. Smith. Expert elicitation survey on future wind energy costs. *Nature Energy*, 10.1038, 2016.

[5] Fraunhofer. Global leading offshore wind power companies in 2017, based on market share. On the WWW, June 2018.

[6] Siemens Gamesa Renewable Energy. Products and services - offshore. On the WWW, June 2018. https://www.siemensgamesa.com/en-int/products-and-services/offshore.

[7] MHI Vestas. Turbines innovation. On the WWW, June 2018. http://www.mhivestasoffshore.com/innovations/.

[8] Morten Thtt Andersen. *Floating Foundations for Offshore Wind Turbines*. PhD Thesis, Aalborg University, Aalborg, DK, September 2016.

[9] J. Jonkman, S. Butterfield, W. Musial, and G. Scott. Definition of a 5-MW Reference Wind Turbine for Off. NREL/TP-500-38060 1, NREL, Golden, CO, February 2009.

[10] Christian Bak, Frederik Zahle, Robert Bitsche, Taeseong Kim, Anders Yde, Lars Christian Henriksen, Anand Natarajan, and Morten Hartvig Hansen. Description of the DTU 10 MW Reference Wind Turbine. DTU Wind Energy Report-I-0092 1, Technical University of Denmark, Kongens Lyngby, DK, July 2013.

[11] DNV. Position Mooring. Offshore Standard DNV-OS-E301, Det Norske Veritas AS, October 2010.

[12] O. M. Faltinsen. *Sea Loads on Ships and Offshore Structures*. Cambridge University Press, 1990.

[13] Zhen Gao. Lecture notes - time-domain equations of motions with convolution terms and their replacement techniques. Technical report, NTNU, 2016.

[14] B. Pereyra, F. Wendt, A. Robertson, and J. Jonkman. Assessment of first- and second-order wave-excitation load models for cylindrical substructures. Number ISOPE-I-16-332, pages 214–219, Rhodes, GR, June 2016.

[15] Line Roald, Jason Jonkman, Amy Robertson, and Ndaona Chokani. Reliability analysis of complex limit states of floating wind turbines. *Energy Procedia*, 35:253–264, 2013.

[16] M. K. Al-Solihat and M. Nahon. Stiffness of slack and taut moorings. *Ships and Offshore Structures*, 11:890–904, 2016.

[17] Lars Bergdahl and Jens Peter Kofoed. Simplified design procedures for moorings of wave-energy converters. Technical report, Aalborg University, 2015.

[18] Henrik Stiesdal. A Floating Wind Turbine and a Method for the Installation of such Floating Wind Turbine. Patent WO/2017/157399, PCT/DK2017/050076, Stiesdal Offshore Technologies A/S, DK, 2017.

[19] A. Pegalajar-Jurado T. Nielsen F. Madsen A. Lomholt R. Mikkelsen M. Mirzaei H. Bredmose, M. Borg. Tetraspar floating wind turbine scale model testing summary report. Technical report, Stiesdal Offshore Technologies, DHI, and DTU Wind Energy, 2017.

[20] M. Karimirad and T. Moan. Feasibility of the application of a spar-type wind turbine at a moderate water depth. *Energy Procedia*, 24:340–350, 2012.

[21] J. Jonkman and W. Musial. Offshore Code Comparison Collaboration (OC3) for IEA Task 23 Offshore Wind Technology and Deployment. NREL/TP-5000-48191 1, NREL, Golden, CO, December 2010.

[22] W. Xue. Design, Numerical Modeling and Analysis of a Spar Floater Supporting the DTU 10MW Wind Turbine. MS Thesis, Norwegian University of Science and Technology, Trondheim, NO, June 2016.

[23] Henrik Bredmose, Michael Borg, Antonio Pegalajar-Jurado, Thomas Raahauge Nielsen, Freddy Johannes Madsen, Anders Kjr Lomholt, Robert Mikkelsen, and Mahmood Mirzaei. TetraSpar Floating Wind Turbine Scale Model Testing Summary Report. Test Report 1, Stiesdal Offshore Technologies, DHI, Technical University of Denmark, Kongens Lyngby, DK, August 2017.

[24] Z. Gao and T. Moan. Mooring system analysis of multiple wave energy converters in a farm configuration. In *8th European Wave and Tidal Energy Conference*, Uppsala, 2009.

[25] IEC. Wind TurbinesPart 3: Design Requirements for Offshore Wind Turbines. International Standard IEC 61400-3, International Electrotechnical Commission, Geneva, CH, February 2009.

[26] DNV. Environmental Conditions and Environmental Loads. Recommend Practice DNV-RP-C205, Det Norske Veritas AS, April 2014.

[27] A Kolios, M Borg, and D Hanak. Reliability analysis of complex limit states of floating wind turbines. *Journal of Energy Challenges and Mechanics*, 2:6–9, 2015.

[28] Mareike Leimeister, Erin Bachynski, Michael Muskulus, and Philipp Thomas. Design optimization and upscaling of a semi-submersible floating platform. 09 2016.

[29] Erin E. Bachynski and Torgeir Moan. Design Considerations for Tension Leg Platform Wind Turbines. *Marine Structures*, 29(1):89 – 114, June 2012.

[30] IRENA. Renewable energy technologies: Cost analysis series - wind power. Technical report, The International Renewable Energy Agency, 2012.

[31] H. Bredmose, F. Lemmer, M. Borg, A. Pegalajar-Jurado, R. F. Mikkelsen, T. Stoklund Larsen, T. Fjelstrup, W. Yu, A. K. Lomholt, L. Boehm, and J. Azcona Armendariz. The triple spar campaign: Model tests of a 10mw floating wind turbine with waves, wind and pitch control. *14th Deep Sea Offshore Wind RD Conference, EERA DeepWind*, January 2017.

[32] Krzysztof Jankowski. Dynamics of double pendulum with parametric vertical excitation. MS Thesis, Technical University of Lodz, Lodz, June 2011.

[33] DNV. DNVGL-ST-N001 Marine operations and marine warranty. Offshore Standard DNVGL-ST-001, Det Norske Veritas AS, June 2016.

[34] MARINTEK. Simo Theory Manual. Theory manual, Sintef, Trondheim, NO, March 2017.

[35] MARINTEK. RIFLEX Theory Manual. Theory manual, Sintef, Trondheim, NO, March 2017.

[36] Orcina. OrcaFlex Help. User manual, Orcina, March 2018. https://www.orcina.com/SoftwareProducts/OrcaFlex/Documentation/Help/.

[37] Anders Myhr, Catho Bjerkseter, Anders gotnes, and Tor A. Nygaard. Levelised cost of energy for offshore floating wind turbines in a life cycle perspective. *Renewable Energy*, 66:714 – 728, 2014.

[38] Zhiyu Jiang, Torgeir Moan, and Zhen Gao. A comparative study of shutdown procedures on the dynamic responses of wind turbines. *Journal of Offshore Mechanics and Artic Engineering*, 137:1–16, February 2015.

[39] Zhiyu Jiang, Madjid Karimirad, and Torgeir Moan. Dynamic response analysis of wind turbines under blade pitch system fault, grid loss, and shutdown events. *Wind Energy*, 17:1385–1409, February 2014.